

BUILDING RESEARCH
ASSN. OF N.Z.
16 NOV 1998
LIBRARY
PRIVATE BAG, PORIRUA, N.Z.

Date: May 1997			



STUDY REPORT

No. 73 (1997)

Seismic Ratings for Residential Timber Buildings

B.L.Deam

RESTRICTED

ISSN: 0113-3675

Preface

This study forms the first of three phases of an investigation of the mechanisms by which degrading framed buildings resist earthquake attack, to enable rational engineering design procedures to be developed for such systems. The second phase will investigate how the the earthquake spectra published in NZS 4203 may be used for degrading structures which exhibit 'slack' inelastic dynamic responses. The third phase will develop a 'pseudo-dynamic' laboratory test regime to assess the behaviour of a laboratory specimen subjected to a slowed-down earthquake ground motion record. The second and third phases will be described in a subsequent report.

Acknowledgments

The author acknowledges the financial support for this study from the Building Research Levy and the Public Good Science Fund of the Foundation for Research, Science and Technology.

SEISMIC RATINGS FOR RESIDENTIAL TIMBER BUILDINGS

BRANZ Study Report SR 73
B.L.Deam

REFERENCE

Deam, B.L. 1997. Seismic Ratings for Residential Timber Buildings. Building Research Association of New Zealand, Study Report SR 73, Judgeford, Wellington, New Zealand.

ABSTRACT

Timber framed structures generally survive earthquakes well because of their intrinsically lighter mass. This survival occurs through load sharing between the large number of elements making up the structure, through having redundant elements, and because the elements are able to deform during an earthquake. The mechanics of load sharing and deformation mechanisms need to be determined if domestic and low-rise light timber framed structures are to be engineered to allow for this enhanced performance.

Reverse cyclic laboratory experimental regimes are used to evaluate the performance of building elements. A computerised system is presented in this report which enables an accurate computer model to be matched to the test element response. Once matched, the model may then be used to analyse the performance of the element under dynamic seismic loading and to generate seismic response spectra. The computer model is shown to provide an excellent match to both reverse cyclic and shaketable laboratory experiments.

A procedure for determining the greatest mass able to be restrained by the element during a design level earthquake is described and applied to New Zealand house pile foundation systems (from experiments described elsewhere) and to a pair of 4.8 m long by 2.4 m high light timber framed walls.

Contents	Page
1. INTRODUCTION	1
2. STRUCTURAL ELEMENTS	2
3. TIME-HISTORY ANALYSIS	6
3.1 Response Spectra.....	6
3.2 Uniform Risk Spectra.....	8
4. PINCHED HYSTERETIC LOOP MATCHING AND ANALYSIS SYSTEM	10
5. VERIFICATION OF PHYLMAS	15
6. SEISMIC MASS RATING PROCEDURE.....	21
7. APPLICATION	22
7.1 Foundation Piles.....	22
7.2 Plasterboard Walls	26
7.3 Summary	28
8. OVERALL SUMMARY AND CONCLUSIONS.....	28
9. RECOMMENDATIONS FOR FURTHER RESEARCH.....	29
10. REFERENCES	30
APPENDIX A: USER MANUAL FOR PHYLMAS PROGRAM.....	32
A1. Installing PhylMas.....	32
A2. Program Description	33
A2.1. Program Screen.....	33
A2.2. Analysis Controls.....	34
A2.3. Menus	35
A3. Modelling the Experimental Data	35
A4. Setting up the Earthquake Record Library	37
A5. Source Code	38
APPENDIX B: LONG WALL ASSESSMENT PROGRAMME	39
B1. Specimen Deformation.....	43
B2. Specimen LW1	45
B2.1. Specimen LW1 Construction.....	45
B2.2. Specimen LW1 Schedule.....	45
B2.3. Specimen LW1 Description.....	47
B2.4. Specimen LW1 Results.....	48
B3. Specimen LW2.....	49
B3.1. Specimen LW2 Construction.....	49
B3.2. Specimen LW2 Schedule.....	51
B3.3. Specimen LW2 Description.....	51
B3.4. Specimen LW2 Results.....	53
B4. Specimen LW3	57
B4.1. Specimen LW3 Construction.....	57
B4.2. Specimen LW3 Schedule.....	58
B4.3. Specimen LW3 Description.....	59
B4.4. Specimen LW3 Results.....	62

B5.	Specimen LW4.....	64
B5.1.	Specimen LW4 Construction.....	64
B5.2.	Specimen LW4 Schedule.....	64
B5.3.	Specimen LW4 Description.....	65
B5.4.	Specimen LW4 Results.....	67
B6.	Experimental Specimen Comparison.....	68
B7.	Conclusions.....	69
APPENDIX C: PROPRIETARY PRODUCTS USED IN THE RESEARCH.		70

Figures		Page
Figure 1	Vertical lateral load resisting structural elements (Buchanan 1989).....	1
Figure 2	Structure load-displacement responses (Park 1989).....	3
Figure 3	Some element hysteretic behaviour approximations.	4
Figure 4	Bar and spring model (Dean 1994).....	5
Figure 5	Response spectra for some common earthquake records and the uniform risk spectra (NZS 4203:1992): a) Acceleration spectra and b) Displacement spectra.	8
Figure 6	NZS 4203 Basic seismic hazard accelerations (uniform risk spectra) for "normal" soils (SNZ 1992).....	9
Figure 7	Hysteretic loop match between a test record and PhylMas.	11
Figure 8	Load-time and load-displacement responses for the Figure 7 timber pile subjected to the artificially generated NZA earthquake record: a) 0.4 sec period, b) 0.7 sec period.	12
Figure 9	Pile response spectra.....	14
Figure 10	a) Hysteresis loops for Stewart's test specimen (Dean et. al. 1986). Approximations using: b) Stewart's idealisation (Dean et. al. 1986) and c) PhylMas.	15
Figure 11	Time-displacement responses for Stewart's specimen and model (Stewart 1987) and PhylMas.	16
Figure 12	Displacement and acceleration spectra for elastic, elastoplastic and pinched models.	17
Figure 13	Spectra for 10 percent variations of pinched model parameters.....	18
Figure 14	Response spectra for slackness oscillator with 10, 20 and 30 mm initial slackness (5 % of critical viscous damping).	20
Figure 15	Displacement spectra for a plywood shearwall (Dean et al. 1987).....	21
Figure 16	Details of foundation piles (Thurston 1994).	22

Figure 17	Pile hysteresis loops for: a) Test piles and b) PhylMas model.....	23
Figure 18	Displacement and acceleration spectra for timber piles subjected to various earthquakes.....	24
Figure 19	Envelope displacement spectra for timber piles.....	25
Figure 20	Wall hysteresis loops for: a) Test specimens and b) PhylMas model.....	26
Figure 21	Envelope displacement spectra for long wall specimens.....	27
Figure A1	PhylMas program screen.....	33
Figure A2	Analysis controls for: a) 'Static' cycle definition and b) 'Dynamic' time-history analysis.....	34
Figure B1	Long wall specimen details.....	39
Figure B2	Test arrangement for long wall specimens.....	40
Figure B3	Displacement measurement positions for the shearwall specimens.....	41
Figure B4	Test arrangement for long wall specimens: a) Viewed from the framing face and b) Viewed from the plasterboard face.....	42
Figure B5	Shearwall deformation modes.....	44
Figure B6	Additional lateral force from gravity load for 50 and 35 mm stud widths.....	45
Figure B7	Deformed shape of framing at +30 mm top plate lateral displacement.....	46
Figure B8	Sectional plan view of wall base showing plasterboard separating from bottom plate.....	47
Figure B9	Framing face of plasterboard after test.....	48
Figure B10	Load-displacement response of Specimen LW1.....	48
Figure B11	Construction details for Specimen LW2.....	50
Figure B12	Stud curvature in Specimen LW2 at a +60 mm displacement.....	52
Figure B13	Specimen LW2 at the end of the test (+290 mm displacement).....	53
Figure B14	Load-displacement responses of Specimen LW2 during cyclic loading and the push to failure.....	54
Figure B15	Lateral displacements compared to those arising from nailslip only.....	56
Figure B16	Construction details for Specimen LW3.....	57
Figure B17	Specimen LW3 during cycles -13 (upper) and +14 (lower).....	60
Figure B18	Specimen LW3 at the end of the test.....	61
Figure B19	Load-displacement response of Specimen LW3.....	62
Figure B20	Specimen LW4 at: a) 60 mm and b) 120 mm displacement.....	66

Figure B21	Load-displacement response of Specimen LW4.	67
Figure B22	Load-displacement response envelopes for Specimens LW1 to LW4.....	68

Tables		Page
Table 1	PhylMas parameters for Figure 16 foundation piles.....	22
Table 2	Pile ratings from Figure 18 periods.	26
Table 3	PhylMas parameters for long walls.	27
Table 4	Wall mass ratings from Figure 21 periods.....	28
Table B1	Shearwall Test Specimen Detail Summary.	40
Table B2	Specimen LW1 Test Schedule.....	46
Table B3	Perimeter Plasterboard Nailslip for Specimen LW1.	49
Table B4	Specimen LW2 Test Schedule.....	51
Table B5	Perimeter Plasterboard Nailslip for Specimen LW2.	55
Table B6	Specimen LW3 Test Schedule.....	58
Table B7	Perimeter Plasterboard Nailslip for Specimen LW3.	63
Table B8	Specimen LW4 Test Schedule.....	64
Table B9	Perimeter Plasterboard Nailslip for Specimen LW4.	67

1. INTRODUCTION

Timber framed structures generally survive earthquakes well (Shephard et al. 1990). This can be attributed to the intrinsically lighter mass of timber structures (which reduces lateral forces) and occurs through load sharing between the large number of elements making up the structure, through having redundant elements, and because the elements are able to deform during an earthquake. The mechanics of load sharing and deformation mechanisms need to be determined if domestic and low-rise light timber framed structures are to be engineered to allow for this enhanced performance.

Most lateral load-resisting structures comprise a combination of the four structural elements shown in Figure 1 (Buchanan 1989). The behaviour of the structure is normally dominated by elements with the greatest stiffness, such as shearwalls, as these attract the greatest loads. The behaviour of the structure will therefore be similar to the behaviour of these principal lateral load resisting elements.

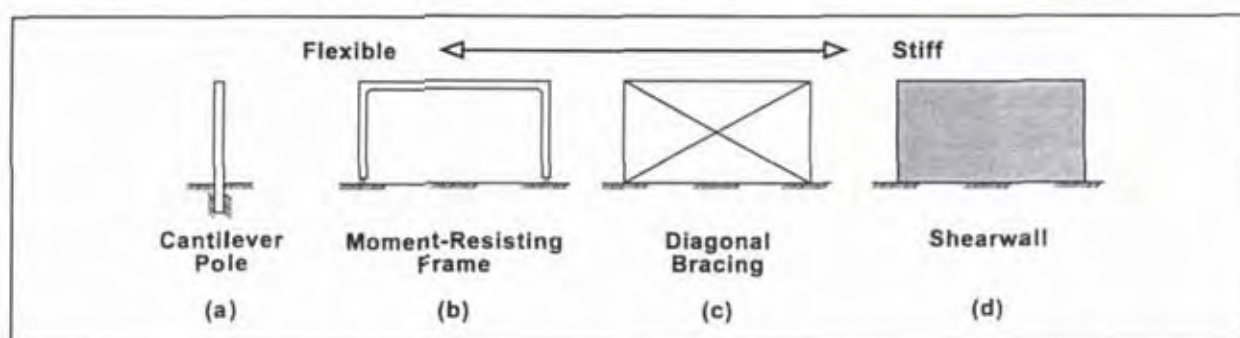


Figure 1 Vertical lateral load resisting structural elements (Buchanan 1989).

The mechanics of the behaviour of lateral load-resisting timber elements subjected to wind are well established and originally formed the basis of design for seismically induced forces (e.g. Stewart 1987). Design for wind generally requires bracing elements to be strong and stiff to resist forces applied to the external building faces during severe storms. The unidirectional nature of these forces is reflected in laboratory test methods (e.g. Reardon 1980) which verify the suitability of structural elements by racking representative specimens in one direction only (monotonic loading). Strength and stiffness are both measured from plots of the applied load and the corresponding specimen deflection.

Seismic design generally requires stiff lateral load-resisting elements to prevent damage during relatively frequent, low-intensity earthquakes. Stiffness may be measured using the unidirectional test method described above. Lateral forces will generally be small compared with those required to withstand less frequent high-intensity earthquakes. The design criterion for high-intensity earthquakes is for the structure to survive the earthquake without collapse, although damage is anticipated (and considered acceptable) in non-structural components and linings as outlined in NZS 4203 (SNZ 1992).

It is uneconomic to design structures to withstand, without damage, the very large forces generated during a high-intensity earthquake. This would require the structure to remain within its elastic limit throughout the event; thus most designers prefer the system to deform inelastically in a controlled manner while avoiding collapse (Dowrick 1977).

This is reflected in laboratory test methods, such as the BRANZ P21 test procedure (Cooney and Collins 1979), which rack elements well beyond acceptable serviceability deflections.

This report proposes a method of rating the capacity of components used for seismic restraint within residential timber buildings. The method matches a numerical model to the observed response of a structural element subjected to reverse cyclic racking. This model is then used to predict the seismic response of the element and to determine the mass that it is able to safely restrain when subjected to a suite of design level earthquakes.

The basis of the numerical model and the seismic analysis technique are outlined in Sections 2 and 3 respectively of this report. The implementation of the model in a computer programme is described in Section 4. The rating method is verified by comparison with a shaketable test response (Section 5) and used to rate both piled foundation systems and plasterboard walls (Section 6). The report is summarised in Section 7 and recommendations for further research are given in Section 8.

2. STRUCTURAL ELEMENTS

The test regime usually employed to assess the degradation of a structural element involves racking the element for a number of cycles to the same deflection in both positive and negative directions, with the magnitude of the deflections incrementing during the test. A plot of the load-deflection history for each reverse cycle applied to the test specimen is called a "hysteresis loop". Hysteresis loops have distinctive shapes which reflect both the material properties and the material arrangements within the element. Hysteresis loops from tests of four different construction materials are reproduced in Figure 2 (Park 1989).

The area bounded by a hysteresis loop can be used as a measure of the energy absorbed by the element as it is cycled (Dowrick 1977). This area is greater for the "fat" hysteresis loops produced by steel and reinforced concrete elements (Figure 2) than for the "narrow" or "pinched" hysteresis loops produced by prestressed concrete and timber elements. Historically it was thought that "pinched" hysteresis loops produced by degrading timber elements, and therefore the elements themselves, were undesirable because less energy was dissipated than by concrete or steel elements (Park 1989). This is clearly inconsistent with the low damage ratio experienced by timber buildings. Thus some other rationale is required to explain the good performance of timber framed systems.

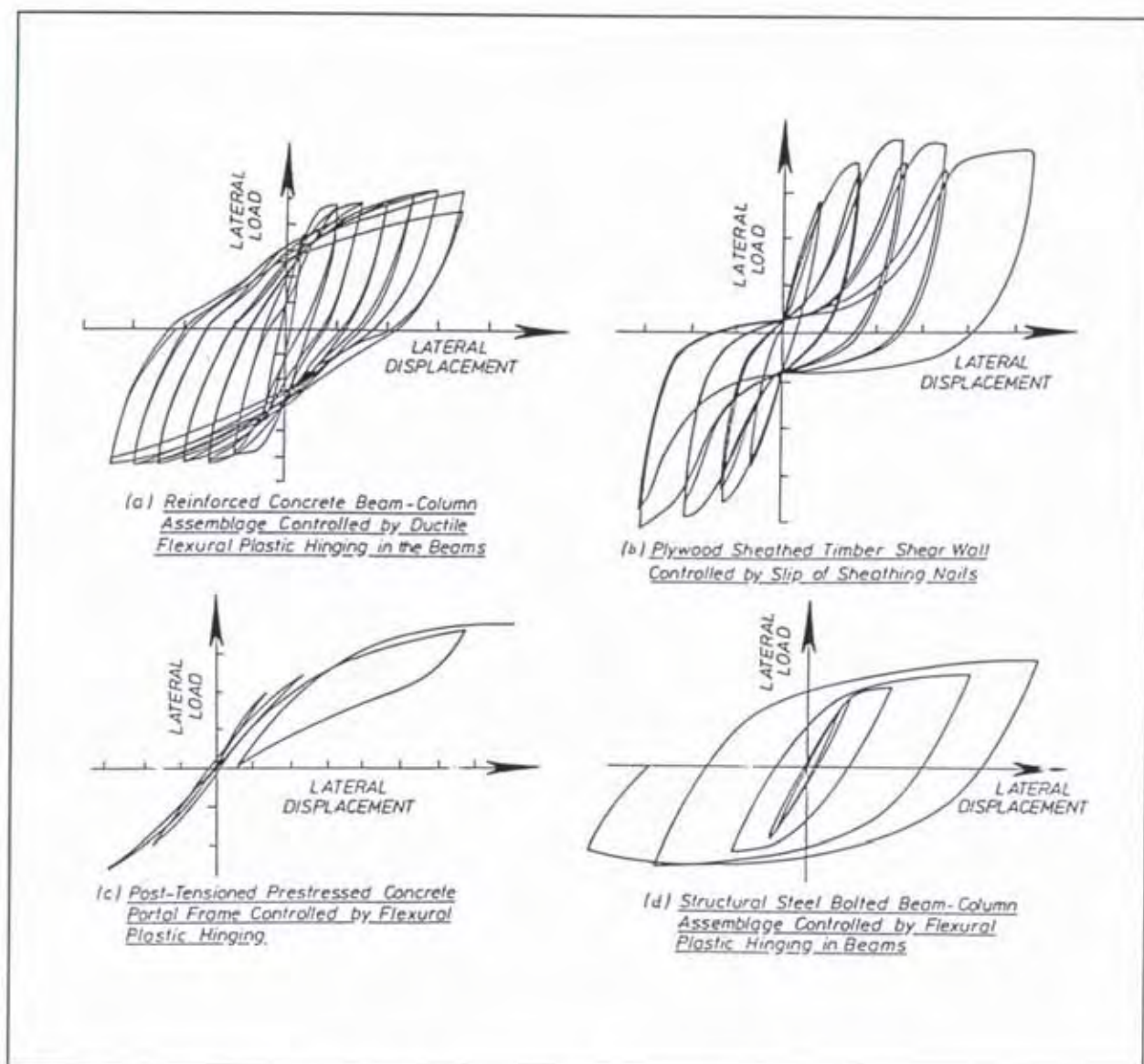


Figure 2 Structure load-displacement responses (Park 1989).

Reverse cyclic testing of structural elements demonstrates the displacement the element is able to withstand. However, to analyse the behaviour of complete structures, designers currently approximate the true hysteretic behaviour of the component elements to simplify the analysis.

The simplest approximation to a hysteresis loop is to assume that the element is perfectly elastic and sustains no damage. Brittle elements are normally assumed to exhibit elastic behaviour, as are elements being analysed for serviceability, i.e. lower magnitude, earthquakes. While this approach provides assurance for 'design code intensity' events, it may not provide reserves for events of marginally greater intensity. The load-displacement response of an elastic element supporting and laterally restraining an arbitrary mass is shown in Figure 3(a).

Non-linear behaviour of structural elements is frequently approximated by the ideal elastoplastic response illustrated in Figure 3(b). This response is a well-established

approximation to hysteresis loops produced by concrete and steel structures and is the basis of many of the world's seismic design codes (e.g. Clough and Penzien 1975).

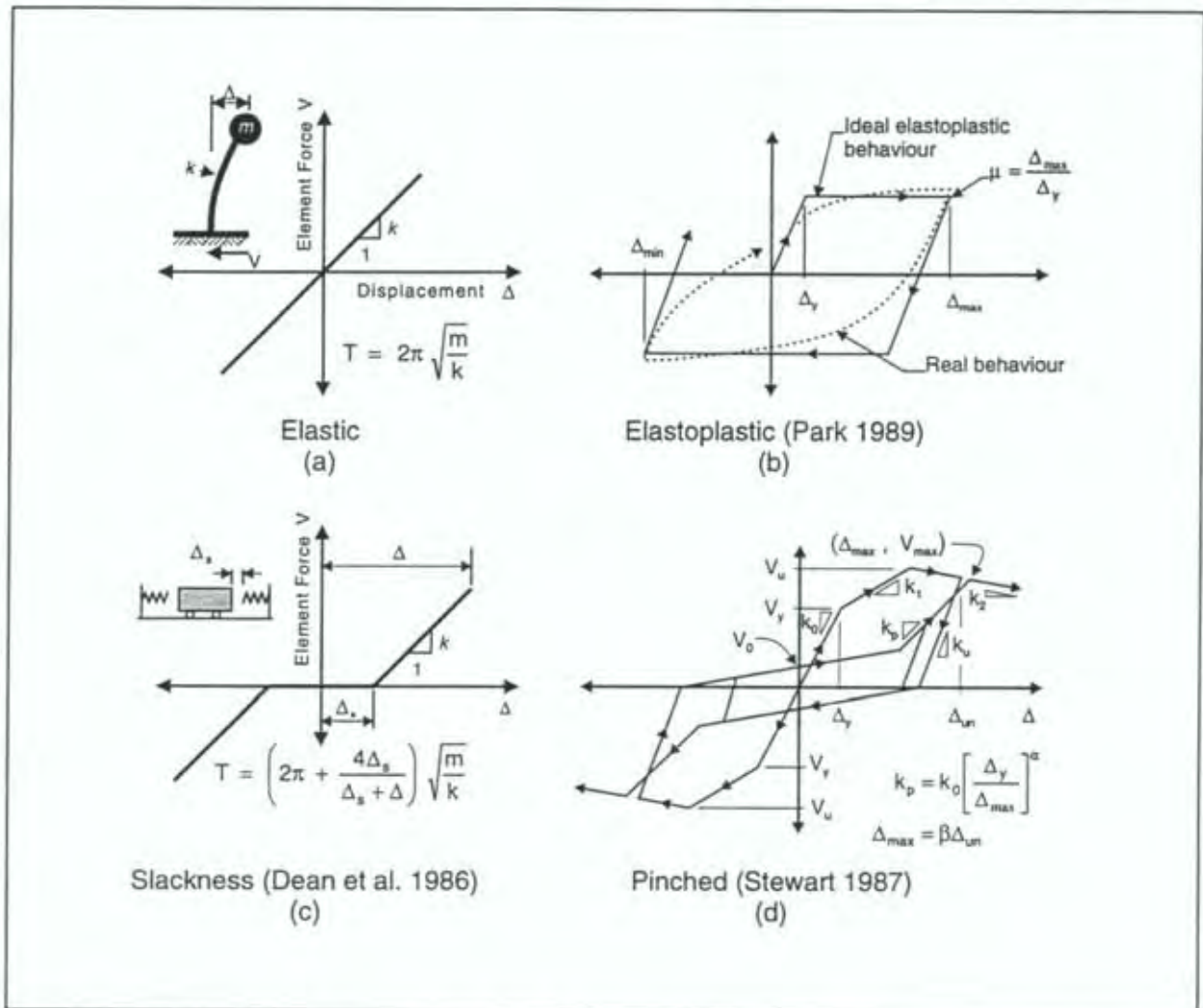


Figure 3 Some element hysteretic behaviour approximations.

A number of methods have been used to fit the elastoplastic approximation to actual hysteresis loops of steel and concrete elements (Park 1989) since in real elements there is no distinctive point at which the onset of plastic deformation (yielding) occurs. However, the elastoplastic response is a poor approximation for modelling degrading (timber) elements.

Dean et al. (1986) suggested that a model comprising a mass oscillating between two linearly elastic springs (i.e. the Figure 3(c) inset) could be used to model pinched hysteresis loops of degrading elements at large displacements. This "slackness oscillator" models the element behaviour when slackness, normally present after the first major ground movement during an earthquake, is developed. However, it does not account for the residual load at zero displacement observed in test records.

Stewart (1987) proposed a hysteretic model which incorporated the pinching effect observed in racking tests conducted with timber elements. This model (Figure 3(d)) used sets of rules to define a tri-linear approximation of the envelope of the load-displacement response and the pinching effects which develop during repeat loading.

The model was developed for plywood shearwalls but can also represent other degrading structural elements.

Dean (1994) proposed a hysteretic model comprising a rigid bar with a number of nominally bi-linear elastoplastic springs attached to it, as shown in Figure 4(a). This model generates the most realistic load-displacement response for timber elements, complete with smooth stiffness transitions as shown in Figure 4(e). The response is able to be modified by altering the characteristics of the springs, with a specified portion of the springs being allowed to develop slackness as they are cycled. The model accurately reproduces the behaviour of a range of structural sub-assembly and system responses. Realistic hysteresis loops can be generated for displacements up to the maximum test displacement but beyond this the model should not be used, as alternative failure mechanisms may develop causing dramatic behaviour changes.

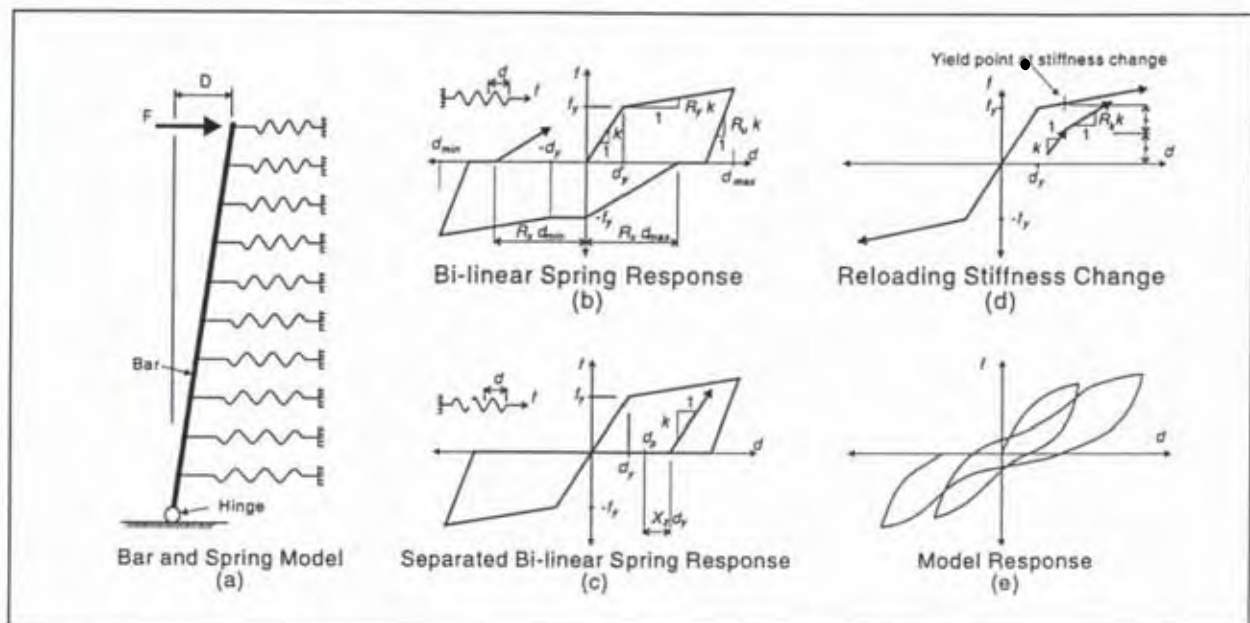


Figure 4 Bar and spring model (Dean 1994).

The rigid bar in Dean's (1994) model is hinged at the base and bears upon ten springs, as shown in Figure 4(a). In use, the top of the bar is displaced by distance, D . The force, F , required for static equilibrium is then calculated from the forces applied to the bar by the ten springs. The springs have the bi-linear force-displacement response envelope shown in Figure 4(b) but some may be springs which develop slackness (Figure 4(c)). The number of bi-linear springs is specified (by a parameter J_p) and the remainder of the springs are separated. The arrangement of the springs produces smooth stiffness transitions without a set of complex mathematical rules, as required by other models.

The separated springs (Figure 4(c)) have the same bi-linear envelope but develop slackness when unloaded. The slackness displacement is related to the maximum displacement during previous cycles. The stiffness of both spring types is able to change when the load increases beyond half the yield load at that displacement, as shown in Figure 4(d), allowing more accurate modelling of test hysteresis loops.

The spring stiffness, yield force and other ratios described above are termed "generating parameters" and may be varied so the model load-displacement response matches the response from a reverse-cyclic pseudo-static specimen test. The computer program

developed for the current study allows the generated load-displacement response to be superimposed over the test specimen response on the computer screen, enabling the generating parameters to be rapidly assessed. Once matched, the generating parameters may be used to model the specimen response for a range of different earthquakes and associated masses using time-history analysis.

3. TIME-HISTORY ANALYSIS

The elastic and non-linear hysteresis models described above are able to predict the stiffness of a lateral load-resisting element. This allows the models to be used in a time-history analysis to simulate the behaviour of the load-resisting element during an earthquake. Single-degree-of-freedom oscillators, as in the Figure 3(a) inverted pendulum, are used to characterise the behaviour of the complete structure (Clough and Penzien 1975).

The behaviour of the Figure 3(a) inverted pendulum is influenced by the restrained mass, m , the stiffness of the support element, k , a viscous damping coefficient, c , and the earthquake acceleration, a_g , at the base. The equation of motion for the pendulum, accounting for each of these components, is given by Equation 1 (Clough and Penzien 1975):

$$ma + cv + kx = -ma_g \quad (1)$$

where a , v and x are the acceleration, velocity and displacement of the restrained mass (relative to the base) respectively.

The base acceleration, a_g , varies with time and Equation 1 is satisfied for each time-step of a recorded or artificially synthesised earthquake acceleration record. The numerical solution process is commonly termed "time-history analysis" because it produces a solution at each time step within the analysed time.

The restrained mass and viscous damping are normally assumed to remain constant throughout the analysis but the stiffness of the structural support element is often permitted to vary, simulating the onset of damage. Further, the viscous damping coefficient, c from Equation 1, is normally given as a percentage of critical damping, c_{cr} , which is calculated from the restrained mass, m , and the initial stiffness, k , using the following equation:

$$c_{cr} = 2\sqrt{mk} \quad (2)$$

3.1 Response Spectra

The maximum force and displacement induced in a structural element during the time-history analysis are usually used to characterise the behaviour of the element. The maximum force is used in the design process to ensure that an element has sufficient strength to restrain the building mass. The maximum displacement, which should not be greater than the maximum test displacement as described previously, is used to limit damage to non-structural components and to ensure that other secondary effects are controlled (i.e. the structure remains stable).

The maximum force and displacement for linear elements can be shown (Clough and Penzien 1975) to be a function of the natural period, T , which, for an elastic structural element (Figure 5(a)), is related to the stiffness, k , of the element and the restrained mass, m , by Equation 3:

$$T = 2\pi\sqrt{\frac{m}{k}} \quad (3)$$

This relationship is also normally applied to non-linear elements for convenience even though the actual "period of oscillation" varies when there is yielding in or degradation of the element. The initial stiffness is normally used to estimate k with non-linear elements.

The maximum force from a time-history analysis is usually given as a non-dimensional spectral acceleration by dividing the force by the acceleration due to gravity, g , and the restrained mass, m . An acceleration "response spectrum" is generated by performing a number of time-history analyses with incremental increases in natural period and plotting the spectral acceleration from each analysis against the natural period.

As an example, elastic acceleration and displacement spectra were generated for a range of commonly used earthquake records, using the computer program developed for this project (described later). The spectra were generated using an elastic element and are given in Figure 5.

The 1977 Bucharest earthquake is representative of a 'soft soil' with relatively large spectral accelerations and displacements in the 1 to 2 second range. The 1940 El-Centro earthquake represents the acceleration levels found in many of the world's seismic codes, although it is no longer regarded as a 'typical' earthquake record. The 1971 Pacoima Dam earthquake is considered the maximum credible earthquake that would be expected to occur in New Zealand (Carr and Moss 1994) and is characterised by large spectral accelerations for periods of less than 0.5 seconds. The 1966 Parkfield earthquake was recorded close to the epicentre and the peak acceleration occurs at a period of 0.3 seconds.

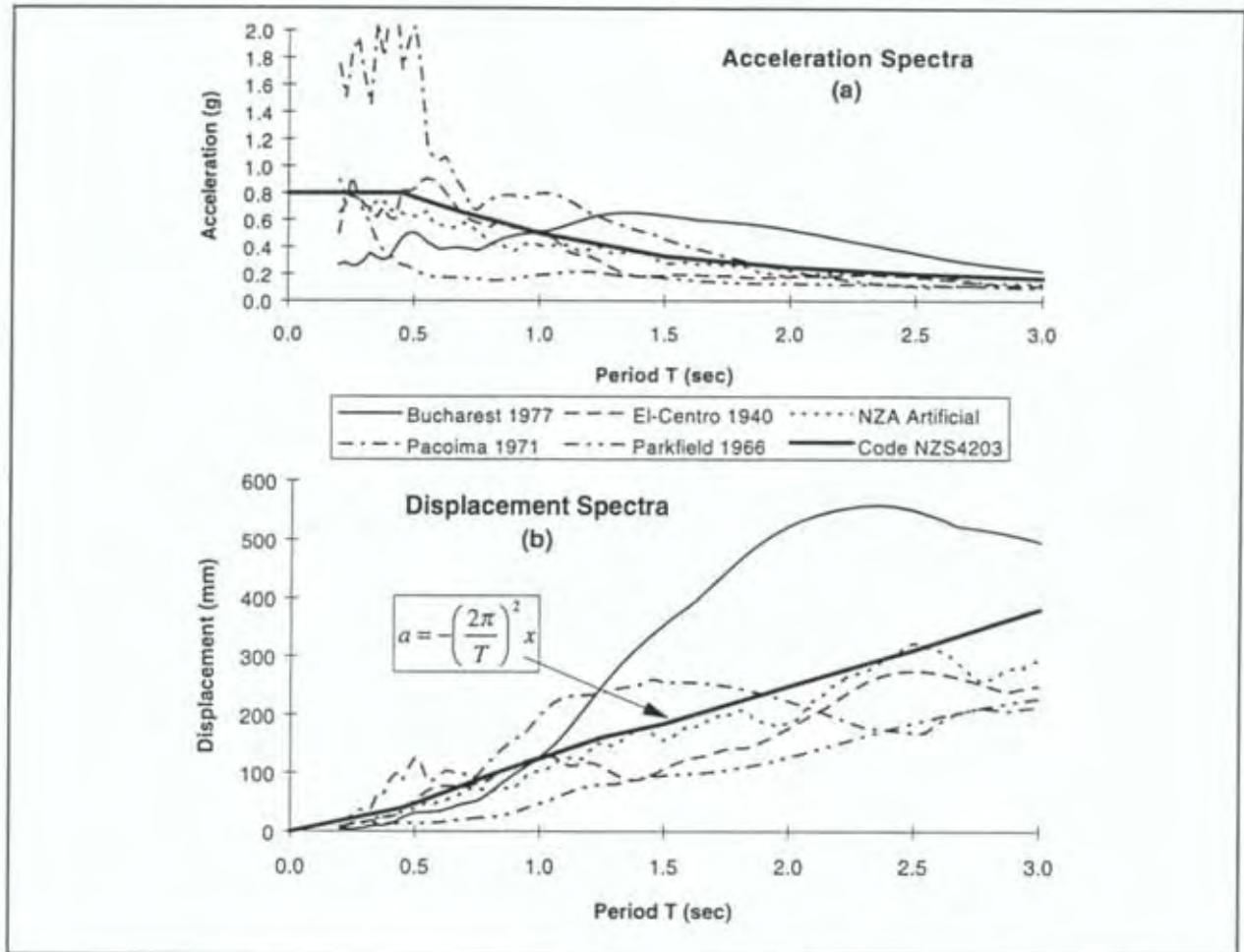


Figure 5 Response spectra for some common earthquake records and the uniform risk spectra (NZS 4203:1992): a) Acceleration spectra and b) Displacement spectra.

3.2 Uniform Risk Spectra

Modern seismic design codes generally give a generic acceleration response spectrum which is modified for specific situations. The New Zealand Loadings Standard NZS 4203 (SNZ 1992) gives a uniform risk acceleration spectrum which is also given in Figure 5. (The elastic displacement spectrum given in Figure 5(b) was derived from the acceleration spectrum using the relationship [Clough and Penzien 1975] given in Figure 5b.) Accelerations given in this spectrum have a uniform (approximately 10%) probability of being exceeded in the given (50 year) time interval across the given range of natural excitation periods when modified to account for the locality of the building.

The most common use of the uniform risk spectra is to estimate "equivalent static" design forces for the building being designed. In use, the elastic natural period, T , of the building is used to determine the acceleration coefficient, $C(T)$, from the uniform risk spectra. This is modified according to the risk (factor R) associated with the building type, the building locality (zone factor Z), the limit state (i.e. ultimate or serviceability), the forces represented (factor L), and a structural performance factor (S_p) which accounts for the fact that "a single peak response of short duration will not necessarily

lead to damage" (NZS 4203, SNZ 1992). (NZS 4203 does not allow the resulting acceleration coefficient to be used for brittle structures which have no inherent reserve strength.) The equivalent static base shear force, V , is obtained by multiplying the appropriately modified spectral acceleration by the building mass, m , and gravity, g , according to Equation 4. The base shear force represents the equivalent static force applied to a single storey building, or is divided between the floors in a multi-storey building.

$$V = C(T)S_p RZL mg \quad (4)$$

An artificial earthquake record (designated NZA) was generated at the University of Canterbury (MacRae 1989) to simulate the uniform risk spectra given in the 1986 draft of the New Zealand Loadings Standard (SANZ 1986). The spectrum for the NZA artificial record is very similar to the NZS 4203 (SNZ 1992) uniform risk spectra when its accelerations are scaled by a factor of 1.25 as shown in Figure 6. This artificial record is useful for time history analyses of New Zealand structures because the accelerations only require scaling by $0.84RZL$, where R , Z and L are the appropriate risk, zone and limit state factors defined above, to subject them to a "code level" earthquake. (This follows the NZS 4203 definition of S_p as 0.67 in Equation 4 above.) The NZA record probably contains more spectral energy than a real earthquake because it matches the uniform risk spectrum from periods of 0.2 to 4.0 seconds. The spectral energy is not spread over such a large period range in real earthquake records.

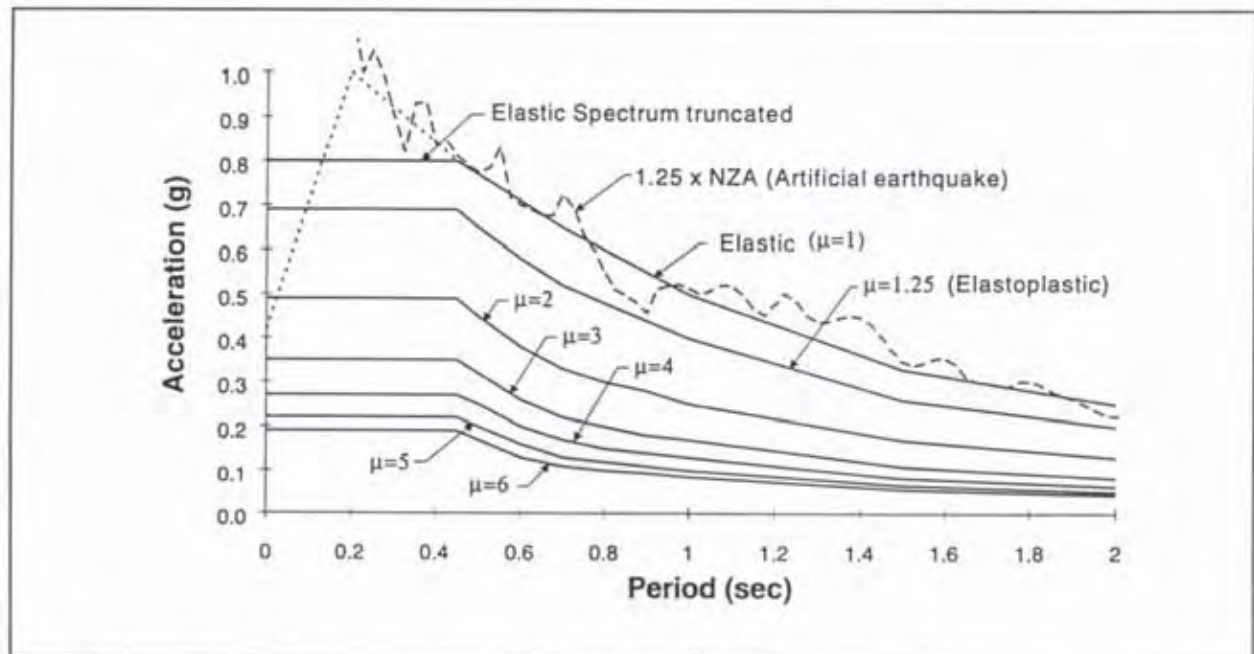


Figure 6 NZS 4203 Basic seismic hazard accelerations (uniform risk spectra) for "normal" soils (SNZ 1992).

Ductility (μ) is commonly used as a measure of inelastic deformation in elements and structures exhibiting elastoplastic behaviour. The ductility used in design is defined as the peak displacement divided by the displacement at yield (Figure 3). The ductility able to be sustained by an element is a function of the materials and their method of construction. It is nominated within the particular materials Standard. (e.g. the Timber Design Standard NZS 3603 [SNZ 1993] for timber elements). The above definition of

ductility, while appropriate for elastoplastic elements, is inadequate for pinched hysteresis elements (such as timber) where no clear yield point can be identified.

Elastoplastic response trades force reduction for greater ductility demand, although the displacement demand usually remains approximately the same as elastic response for periods greater than 1.0 second (NZS 4203, SNZ 1992). (The common rule-of-thumb 'equal displacement demand' is a useful approximation without any rigorous basis.) This is not true for all earthquakes but is used for natural periods greater than one second in many seismic loadings codes, e.g. NZS 4203.

Envelopes of inelastic elastoplastic response spectra are often provided in seismic codes for inelastic design. Spectra are usually given for a range of ductility demands, allowing equivalent static forces to be obtained for a given period and structural ductility as described above for the elastic spectrum. As an example, the elastic and elastoplastic response spectra for normal soils given in NZS 4203:1992 (SNZ 1992) are also reproduced in Figure 6.

4. PINCHED HYSTERETIC LOOP MATCHING AND ANALYSIS SYSTEM

To perform a meaningful time-history analysis, the hysteretic loop approximations require fitting to realistic measured test hysteresis loops. The elastoplastic response (Figure 3(b)) is a poor approximation of the behaviour of timber structures. Stewart's approximation (Figure 3(c)) is better but it too requires curves to be approximated with straight lines. Dean's (1994) bar and spring model gives the best match but is difficult to fit because of the large number of generating parameters. The finite element method has been used by others to model elemental behaviour (e.g. Dolan 1989) but was considered to be too cumbersome because separate models are required for each timber element being analysed.

A computer-based system called "PhylMas" (an acronym of the above section title) was developed to facilitate the generation of appropriate 'generating parameters' for test specimens and to allow time-history analysis to be performed. PhylMas was developed from the computer implementation of Dean's bar and spring model (Dean 1994) but was extensively modified within Microsoft Windows to simplify the user interface and to allow results to be easily processed. Detailed instructions for using the software are given in Appendix A.

PhylMas enables the generating parameters to be quickly adjusted to match test specimen hysteresis loops by graphically superimposing generated and test hysteresis loops on the computer screen. The parameters are varied by movement of the computer's mouse and the generated loops are updated almost instantaneously. Figure 7 shows the excellent match between the smooth hysteresis loops generated by PhylMas and those from the test record of a laterally loaded domestic sub-floor pile.

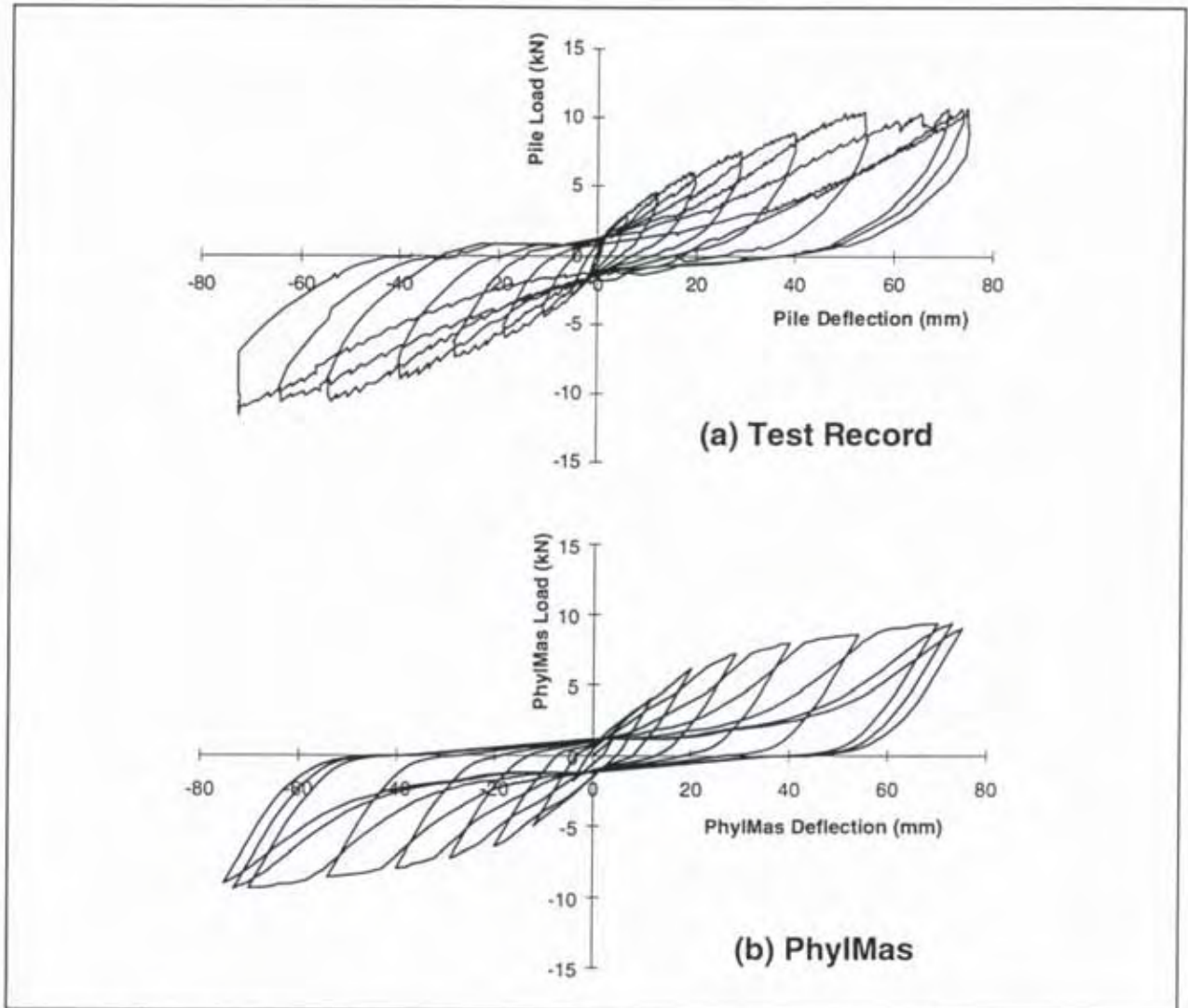


Figure 7 Hysteretic loop match between a test record and PhylMas.

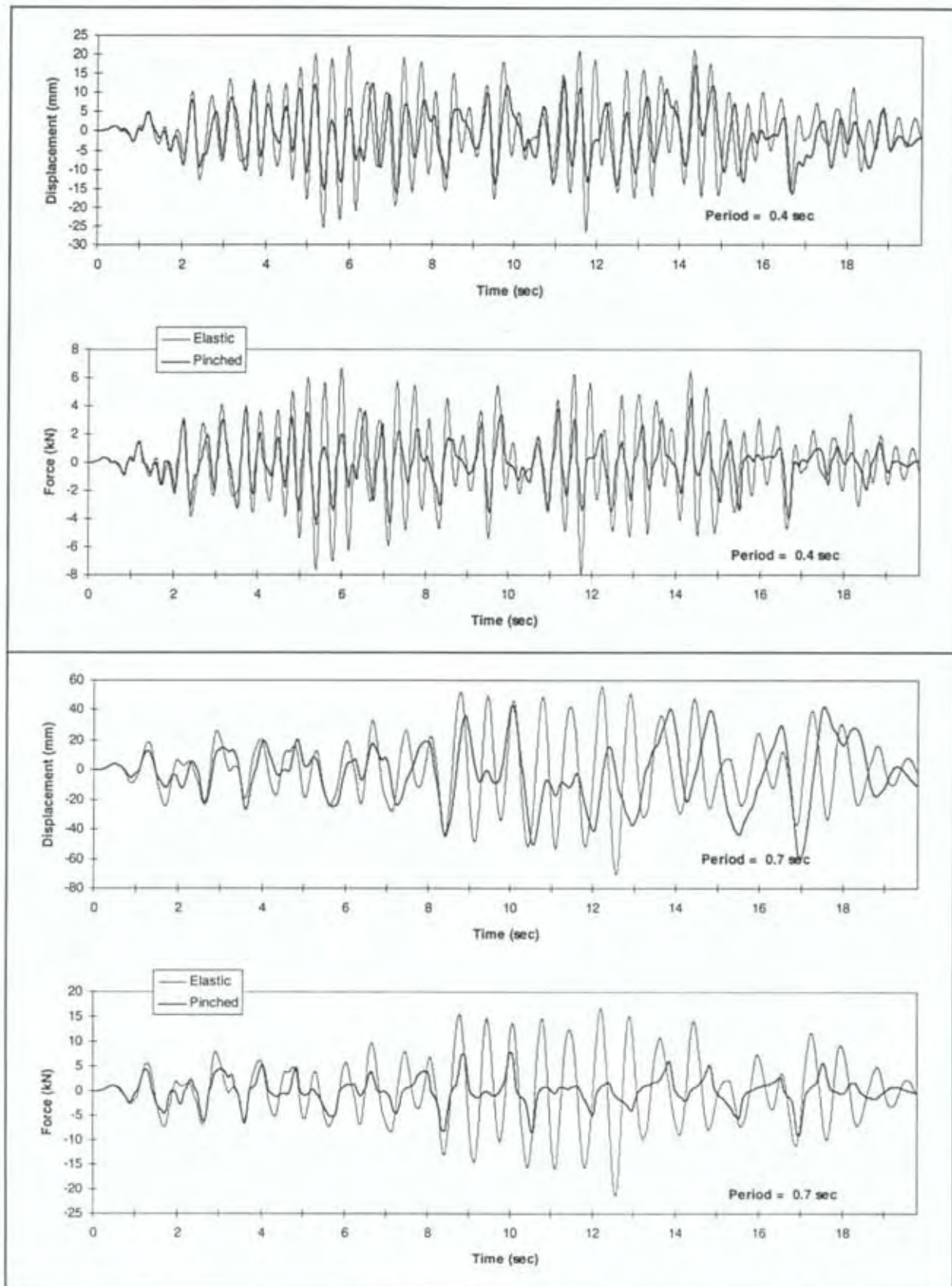


Figure 8 Load-time and load-displacement responses for the Figure 7 timber pile subjected to the artificially generated NZA earthquake record: a) 0.4 sec period. b) 0.7 sec period.

Non-linear time-history analyses are performed within the PhylMas program for a single degree-of-freedom oscillator, using acceleration records from a library of simulated and recorded earthquakes. Hysteresis loops, load-time records and displacement-time records are all able to be displayed and saved for further processing.

Earthquake record accelerations are able to be scaled by multiplying by a constant factor. The natural period is set by the user and specifies the mass restrained by the specimen using Equation 3 and the specimen stiffness k . Load-displacement, load-time and displacement-time responses of the element are able to be plotted on the computer screen or saved for later analysis. Time-history analyses are able to be performed using elastic, elastoplastic and slack models as well as the pinched model.

PhylMas uses the linear acceleration step-by-step method (Clough and Penzien 1975) for the time-history analysis. A relatively small time-step (0.005 sec) is required for the analysis because the stiffness of the pinched model is highly non-linear.

Load-time and load-displacement responses for the Figure 7 timber pile are given in Figure 8 for natural periods of 0.4 and 0.7 sec (i.e. masses of 1210 and 3720 kg respectively). The elastic response is also plotted in Figure 8 for comparative purposes. The time-history analysis was conducted using the artificial NZA earthquake record with a scale factor of 1.0. The viscous damping for this, and the remainder of the analyses reported here, was 5 percent of critical.

The forces in the elastic system are higher. It is also interesting to note that the seismically induced displacements were significantly lower for the pinched system than they were for the elastic system for this analysis.

PhylMas is able to produce acceleration and displacement response spectra by performing a series of time-history analyses, incrementing the natural period (ie the mass) before each analysis. Figure 9 shows acceleration and displacement response spectra generated for three piles subjected to the Figure 6 NZA artificial earthquake record. The general trend for displacement to increase and acceleration to decrease as the period increases are also apparent in Figure 9.

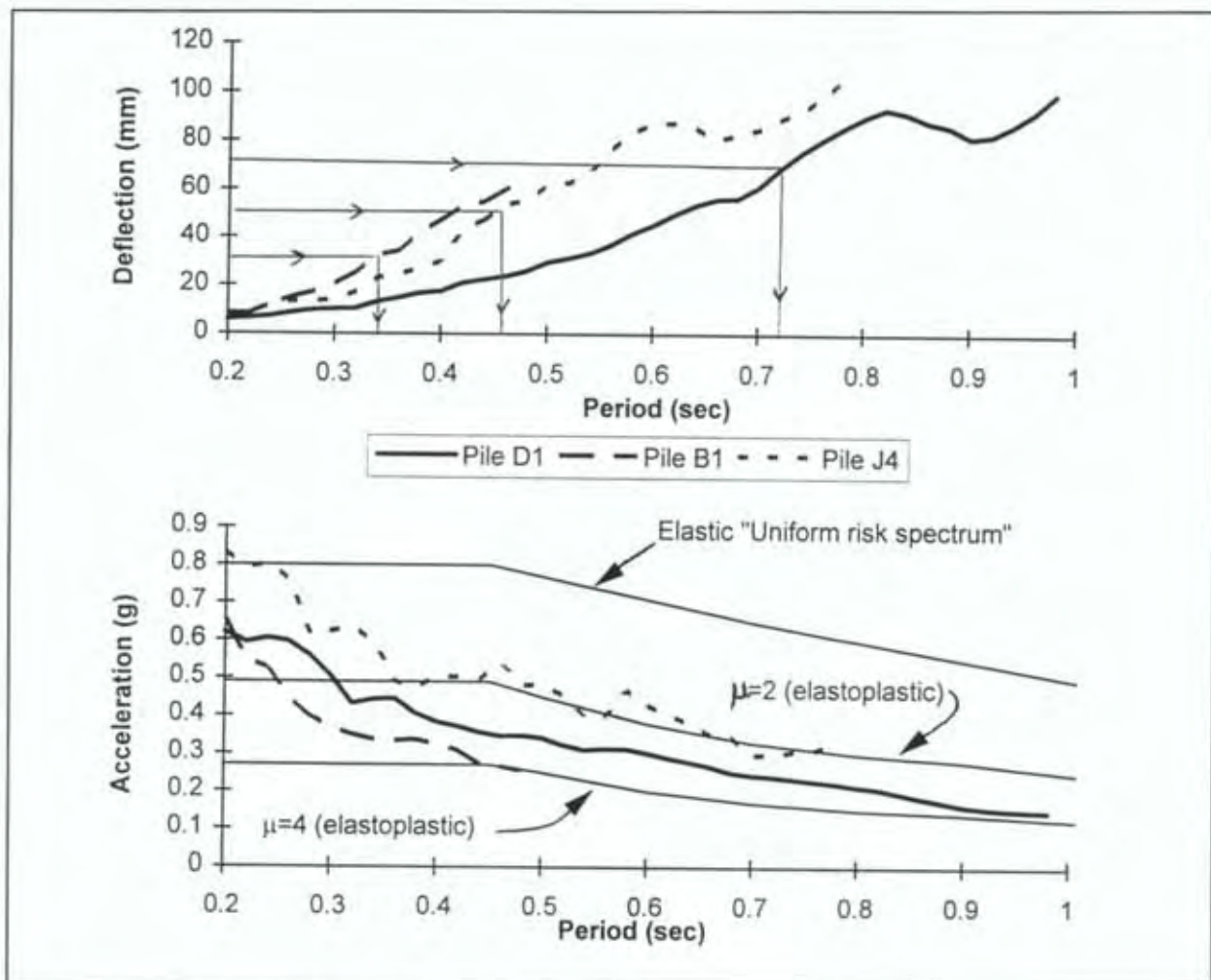


Figure 9 Pile response spectra.

The arrows in the Figure 9 displacement spectrum illustrate how the effective period T is assessed from the maximum test displacement. The mass, m , in kg which the specimen can carry is then determined using Equation 3, rearranged to the following form:

$$m = 25300kT^2 \quad (5)$$

where the initial stiffness k is in kN/mm and the period T is in seconds.

The NZS 4203 (SNZ 1992) uniform risk spectra for elastoplastic ductility levels $\mu=2$ and $\mu=4$ (from Figure 6) are also shown in Figure 9. The pile acceleration response spectra are within the range of $\mu=2$ to $\mu=4$ for periods greater than 0.4 sec, which suggests that these pinched hysteresis loops can be approximated by elastoplastic $\mu=3$. This is lower than the $\mu=4$ used to derive the Code of practice for Light Timber Frame Buildings not requiring specific design NZS 3604 (SANZ 1990).

It is of interest that the pile acceleration spectra approximately follow the elastoplastic spectra such that the equivalent pile ductility is independent of the natural period. This indicates that a particular material or construction may be assigned an 'effective

ductility' for the purpose of calculating design forces. This constant ductility is likely to be of limited use because the yield force remains undefined.

5. VERIFICATION OF PHYLNAS

The accuracy of the PhylMas time-history analysis was verified by comparing a predicted earthquake displacement response with that of a specimen tested on a shake table by Stewart (1987). Stewart conducted quasi-static and shake table tests with identically constructed plywood sheathed timber framed shearwalls. The hysteresis loops for one quasi-static test are reproduced in Figure 10, along with approximations generated with Stewart's model (Figure 3(d)) and PhylMas.

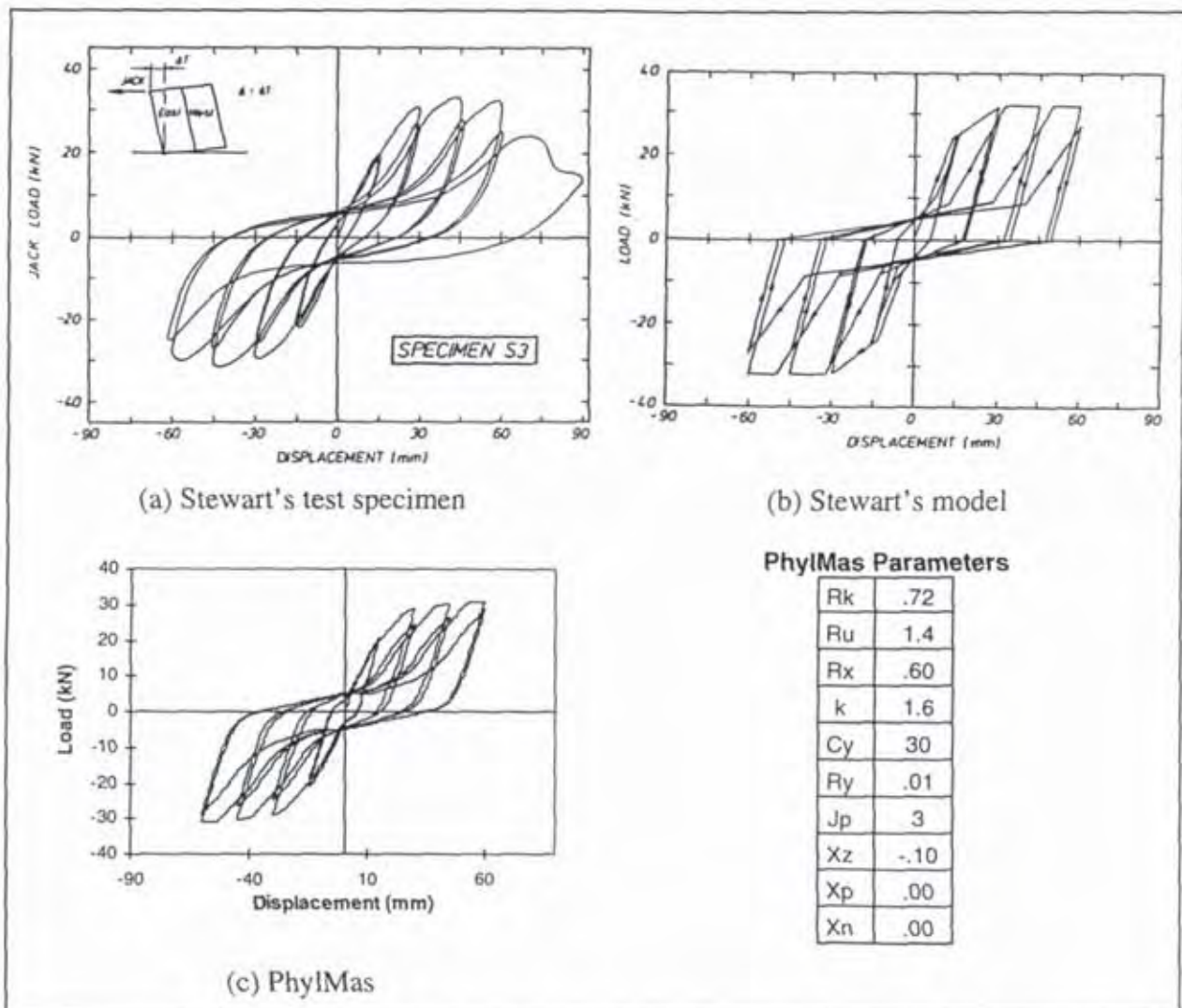


Figure 10 a) Hysteresis loops for Stewart's test specimen (Dean et. al. 1986).
Approximations using: b) Stewart's idealisation (Dean et. al. 1986) and
c) PhylMas.

The displacement-time response from an identically constructed specimen subjected to El Centro 1940 ground motion is reproduced in Figure 11, along with time-history responses predicted by Stewart's model and PhylMas. This shows good agreement between the specimen response and PhylMas prediction even though the shake table was unable to exactly reproduce the ground motion. (The analysis conducted with

Stewart's model used the actual shake table motion whereas the analysis conducted with PhylMas used the original El Centro earthquake). The viscous damping that gave the best match using Stewart's model was 10 % of critical, whereas 14 % of critical gave the best match with PhylMas. (Test specimen damping coefficients measured by Stewart ranged from 7 to 20 %.)

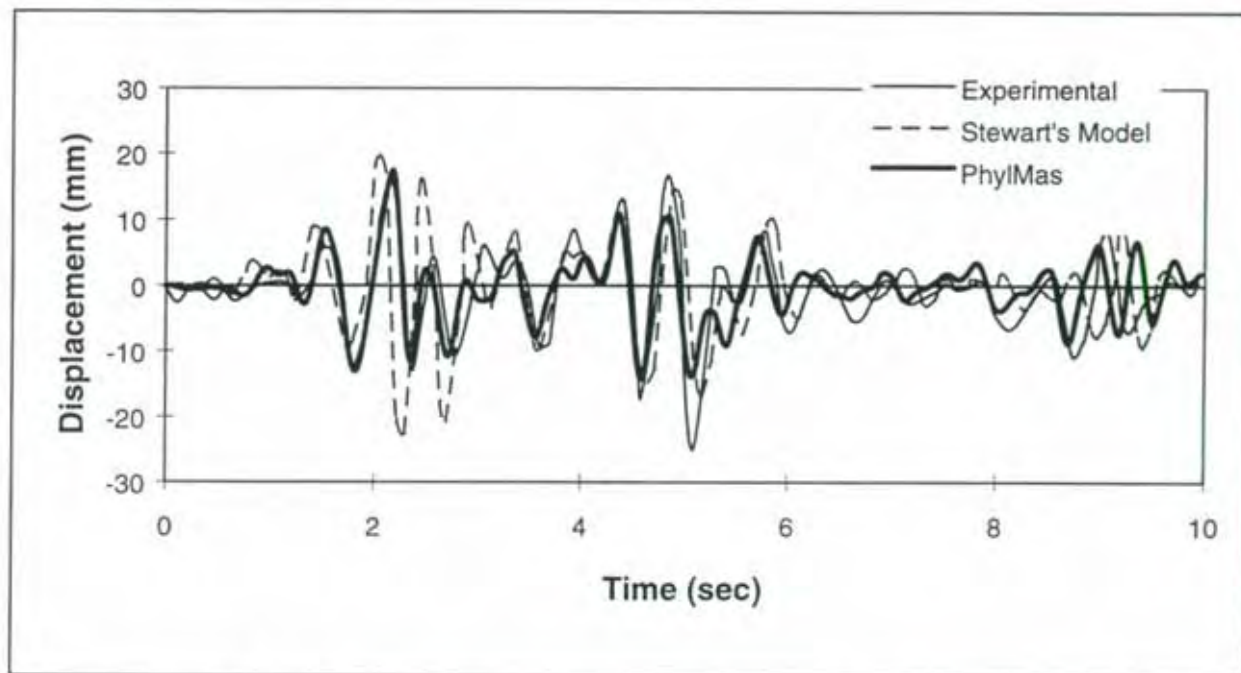


Figure 11 Time-displacement responses for Stewart's specimen and model (Stewart 1987) and PhylMas.

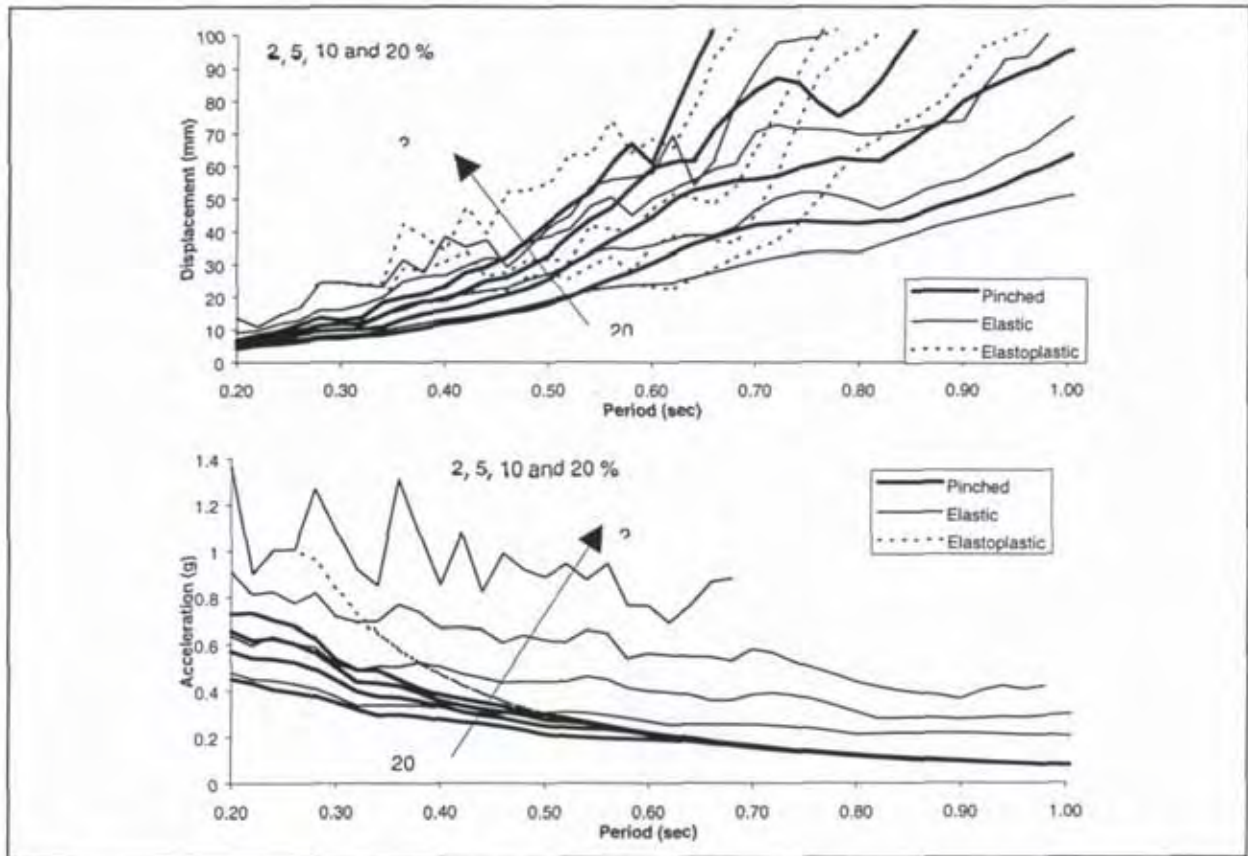


Figure 12 Displacement and acceleration spectra for elastic, elastoplastic and pinched models.

Displacement and acceleration spectra for the elastic, elastoplastic and pinched models were generated using PhylMas at 2, 5, 10 and 20 percent of critical damping. (The same yield force of 30 kN was used for the elastoplastic and pinched models.) The spectra are given in Figure 12 and show that the displacements are approximately the same for the three models but the accelerations are reduced for the pinched model. The acceleration reduction is greater at small natural periods for the pinched model because of hysteretic damping but becomes similar to that of the elastoplastic model for periods of greater than 0.6 sec.

The sensitivity of the pinched model was investigated by generating displacement and acceleration spectra for a series of input parameters. The hysteresis loops of a test specimen (Specimen LW2 described in Appendix B) were matched using PhylMas and then a base response spectrum was generated for the NZA artificial earthquake. Displacement and acceleration response spectra were then generated for (approximately) 10 percent increases and decreases in each parameter. (The parameters are shown in Figure 13 and described in Appendix A.) The spectra in Figure 13 show that displacements are most sensitive to stiffness (Figure 13(d)), intercept force (g) and degradation (h) and that accelerations (i.e. element forces) are most sensitive to stiffness (Figure 13(d)), yield strength (f) and intercept force (g).

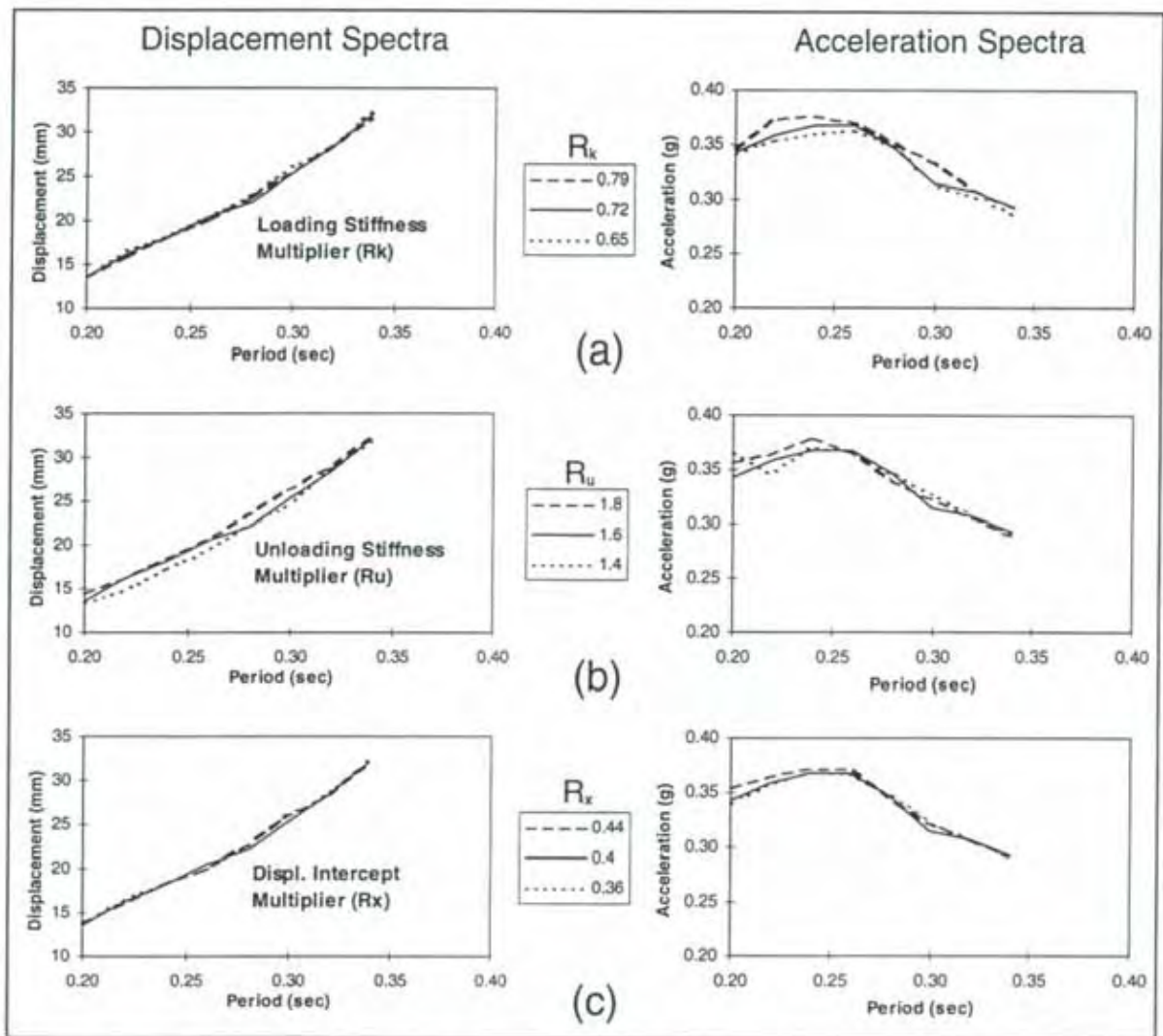


Figure 13 Spectra for 10 percent variations of pinched model parameters.

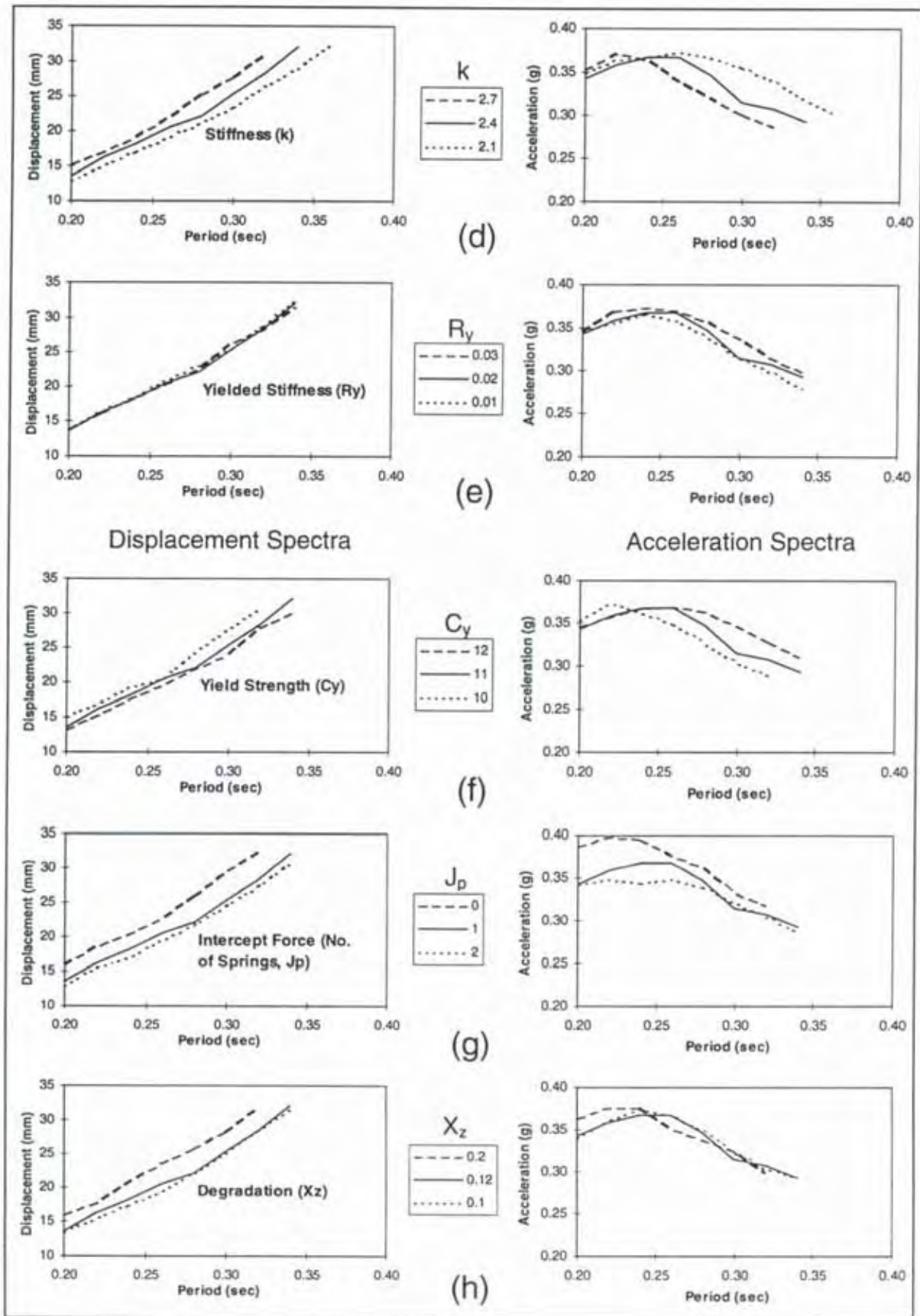


Figure 13 (continued) Spectra for 10 percent variations of pinched model parameters.

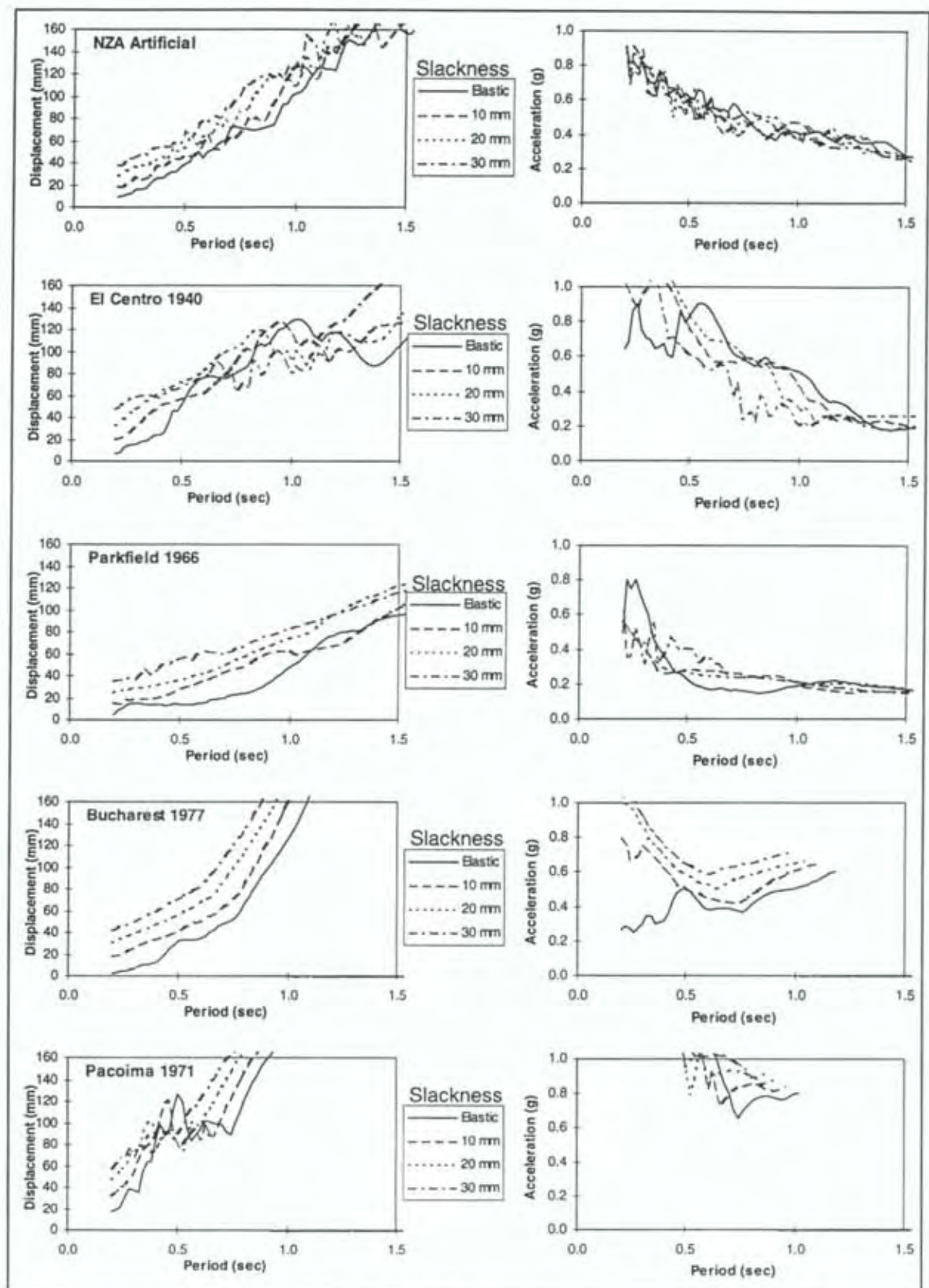


Figure 14 Response spectra for slackness oscillator with 10, 20 and 30 mm initial slackness (5 % of critical viscous damping).

6. SEISMIC MASS RATING PROCEDURE

It has been shown that it is difficult to directly assess both “yield” and “ductile capacity” for degrading structures or elements which have pinched hysteresis loops. An alternative design method, based on displacement, may be employed instead.

Dean et al. (1986) showed theoretically that slackness increases the natural period of oscillation. PhylMas was used to confirm this for a series of earthquakes; the response spectra for 10, 20 and 30 mm initial slackness are given in Figure 14. As the maximum accelerations of most earthquake spectra decrease as the period increases, this effectively reduces the maximum force in the structural element. This force reduction occurs without “fat” hysteretic loops normally associated with absorption of seismic energy. It is of interest that the displacement demand with slackness is similar to that with elastic and elastoplastic behaviour. Slackness is also thought to isolate the mass from high ground acceleration pulses of short duration. However, both accelerations and displacements are increased where the earthquake has more energy at greater periods (e.g. the Bucharest 1977 earthquake as shown in Figure 14).

Dean et al. (1987) used the hysteretic loop approximations for Stewart’s shearwalls to produce envelopes of the displacement response spectra for a range of earthquake records. The response spectra for one shearwall are reproduced in Figure 15. The maximum displacement of the specimen may be used to determine the mass able to be restrained by the shearwall from this envelope curve, without requiring the yield force or ductile capacity of the shearwall to be defined.

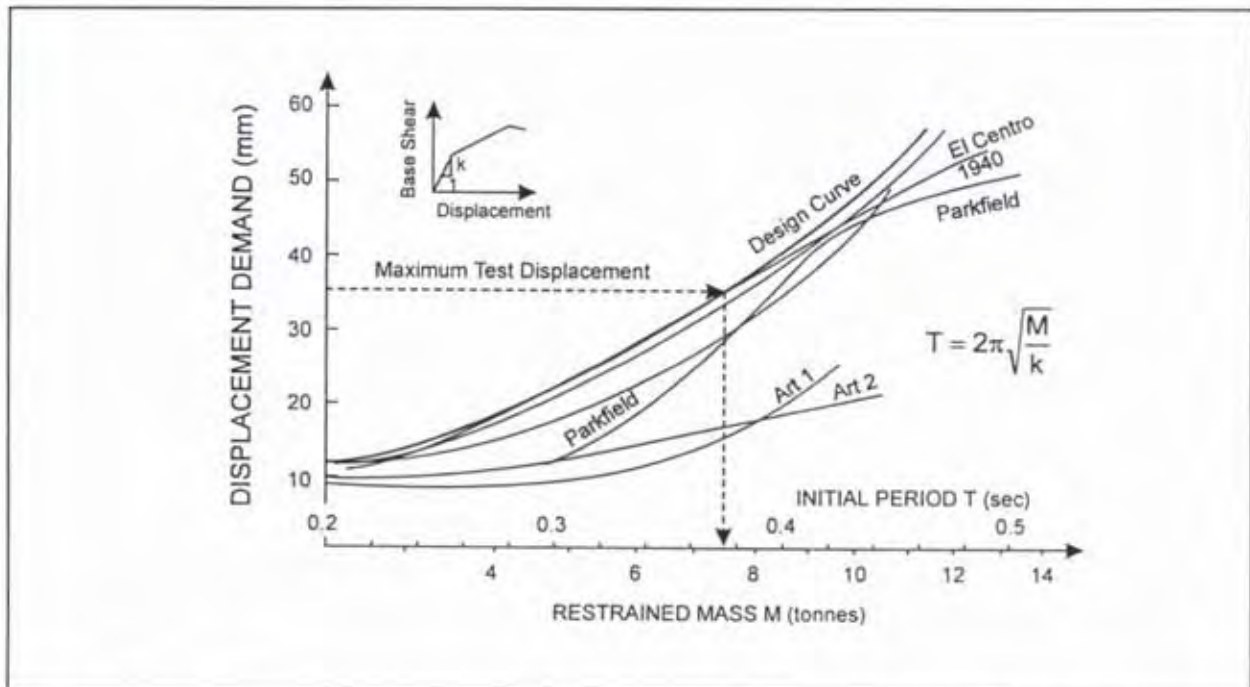


Figure 15 Displacement spectra for a plywood shearwall (Dean et al. 1987).

Thus the following procedure is proposed for obtaining seismic ratings for a timber element using the PhylMas computer program.

1. Match the hysteresis loops of the test specimen being rated.

2. Generate displacement response spectra for a range of earthquake records.
3. Plot the displacement response spectra on a common plot and fit an envelope spectrum. Find the natural period T on this envelope that corresponds to either the maximum displacement of the test specimen or a lesser displacement if required.
4. The mass m able to be restrained by the element may then be calculated from the natural period T , using the stiffness k from the hysteresis loop match and Equation 5.

7. APPLICATION

The seismic mass rating procedure was applied to hysteresis loops from a series of sub-floor foundation piles tested by Thurston (1994) and a series of 4.8 m long light timber framed walls clad with paper faced plasterboard (described in Appendix B). The load-displacement responses of the test specimens were matched and analysed using PhylMas.

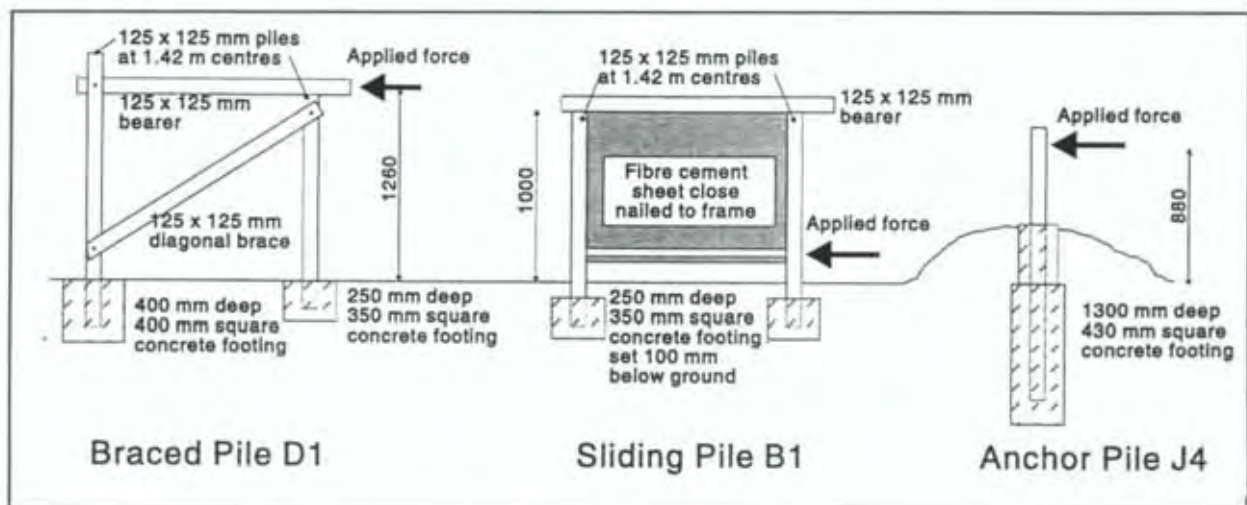


Figure 16 Details of foundation piles (Thurston 1994).

7.1 Foundation Piles

Hysteresis loops from three representative foundation pile tests conducted by Thurston (1994) were selected for analysis using PhylMas. Details of the three piles are given in Figure 16; a complete description of the testing programme is recorded elsewhere (Thurston 1994).

Test and PhylMas generated hysteresis loops are reproduced in Figure 17 for the three piles. The PhylMas parameters are given in Table 1.

Table 1 PhylMas parameters for Figure 16 foundation piles.

Parameter	Rk	Ru	Rx	k	Cy	Ry	Jp	Xz	Xp	Xn
Braced Pile D1	1.6	2	0.6	0.3	7	.16	3	-0.1	0	0
Sliding Pile B1	0.60	1	0.4	2.2	20	.10	1	0.1	0	0
Anchor Pile J4	0.72	1	0.3	0.8	10	.12	2	0.1	0	0

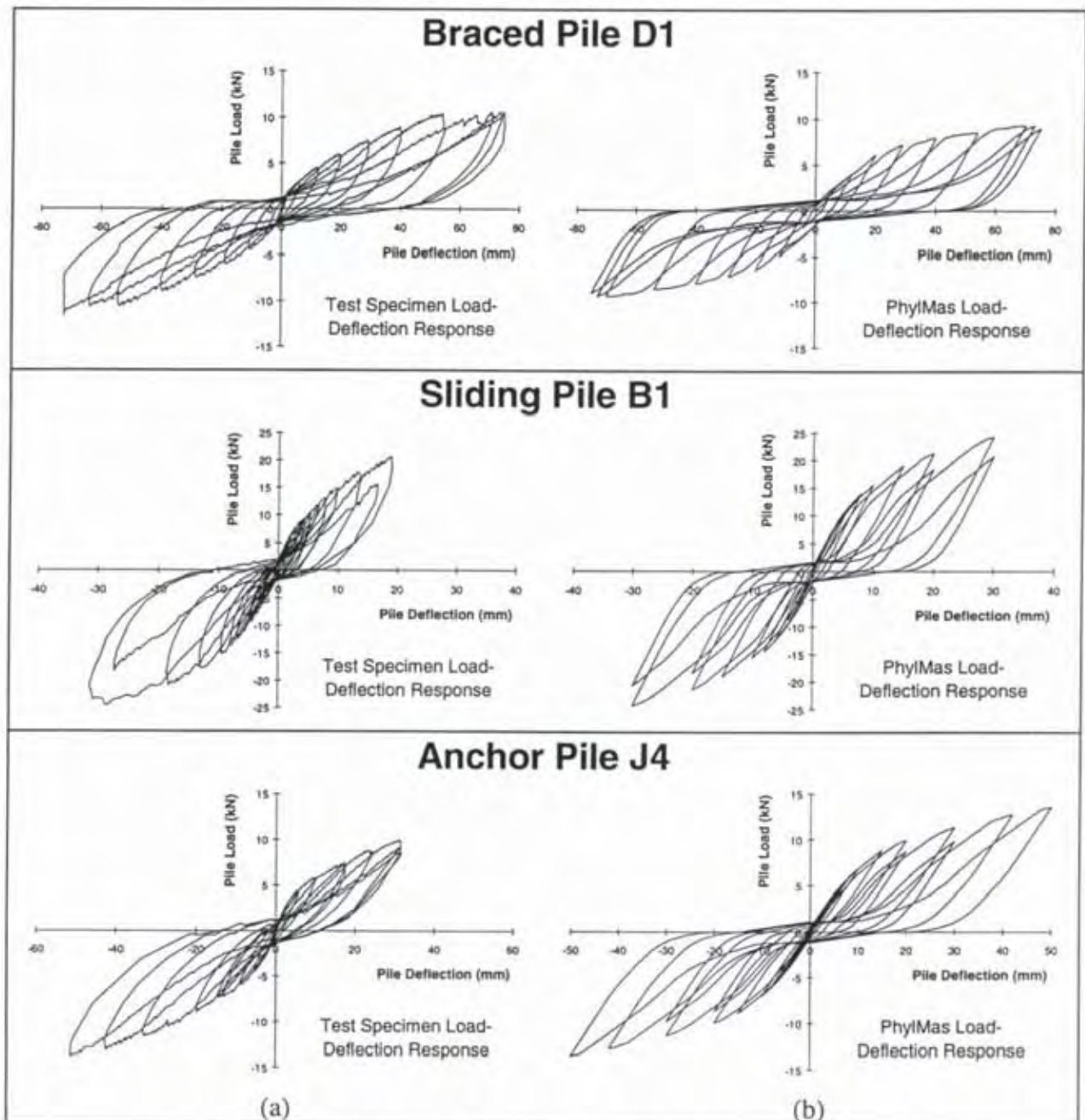


Figure 17 Pile hysteresis loops for: a) Test piles and b) PhylMas model.

Acceleration and displacement spectra were generated for the same five earthquake records used to generate the Figure 5 elastic response spectra. Elastic and inelastic spectra are given in Figure 18 for the three piles for the 5 earthquake records. The earthquake scale factor was 1.0 and the damping was 5 % of critical, as it was expected there would be less damping present than in Stewart's shearwalls. These spectra were generated for displacements up to twice the maximum test displacement.

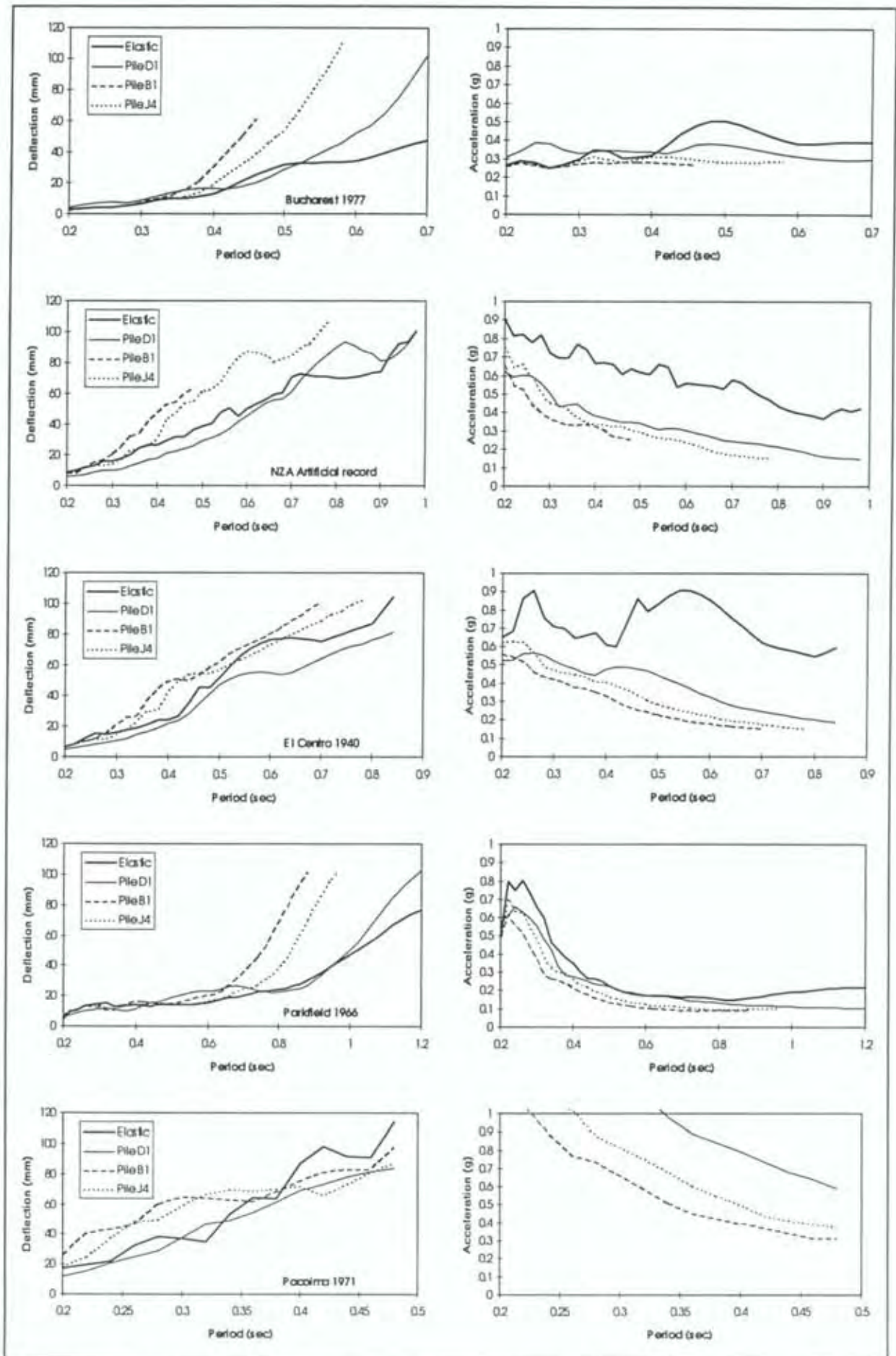


Figure 18 Displacement and acceleration spectra for timber piles subjected to various earthquakes.

The Figure 18 displacement response spectra are given on a common plot for each pile in Figure 19. The response to the Pacoima earthquake was not plotted as it is a maximum credible event (see Section 3.1) whereas the other four are considered more suitable for New Zealand design. An envelope response has also been plotted to determine the maximum period (and hence mass) the pile can resist at the maximum test displacement.

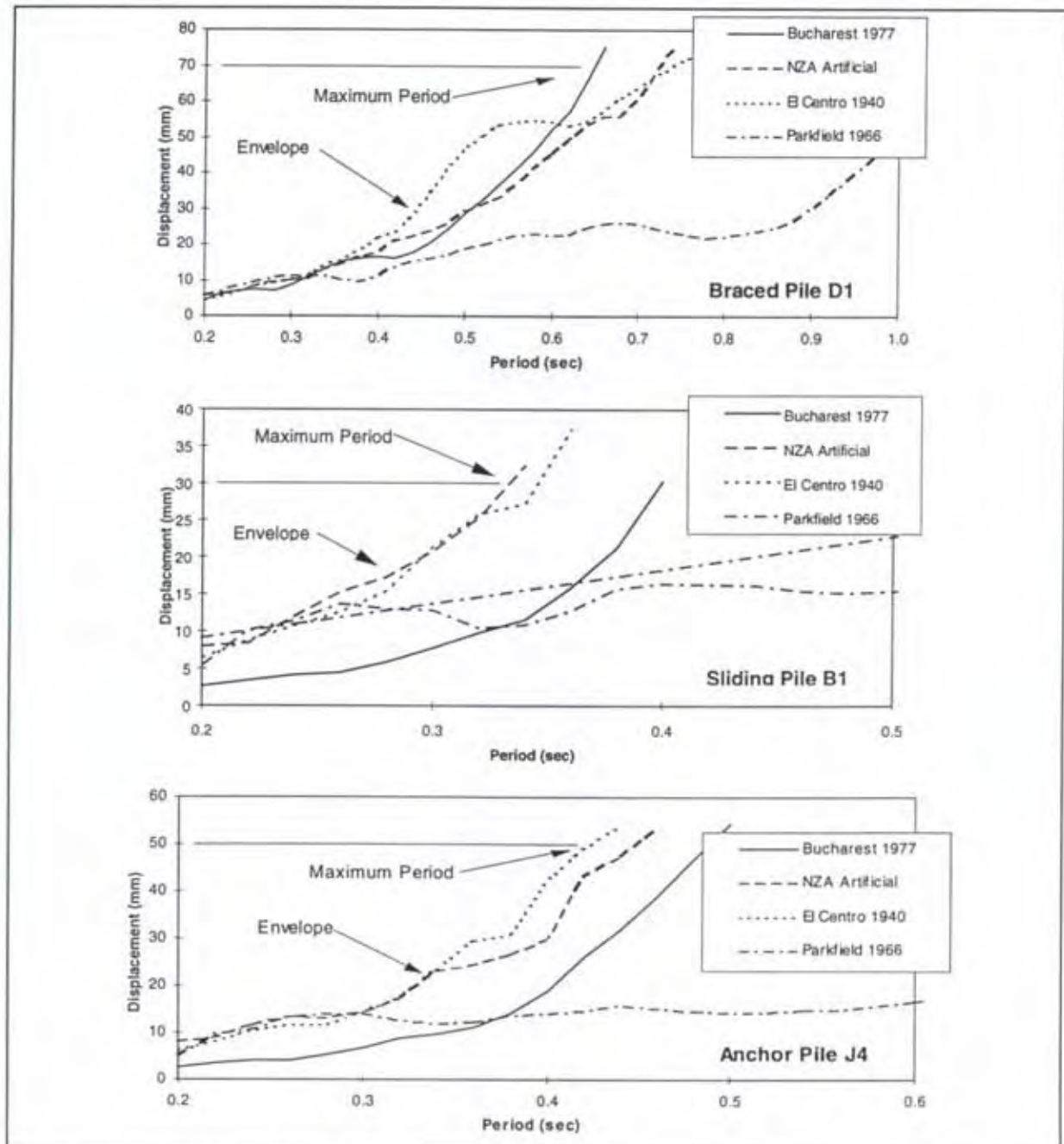


Figure 19 Envelope displacement spectra for timber piles.

The governing earthquakes, the mass ratings (calculated using Equation 5) and the maximum periods from Figure 19 for the three piles are given in Table 2.

Table 2 Pile ratings from Figure 18 periods.

Pile	Limiting Earthquake	Maximum Test Displacement (mm)	Period T (sec)	Stiffness k (kN/mm)	Mass M (kg)
Braced pile D1	Bucharest 1977	70	0.63	0.3	3000
Sliding pile B1	NZA Artificial	30	0.33	2.2	6100
Anchor pile J4	El Centro 1940	50	0.41	0.8	3400

7.2 Plasterboard Walls

Hysteresis loops from two 4.8 m long, 2.4 m high plasterboard sheathed shearwalls were matched using PhylMas. (Full details of the specimens and the testing regimes are given in Appendix B.) The test hysteresis loops and the corresponding PhylMas-generated loops are given in Figure 20.

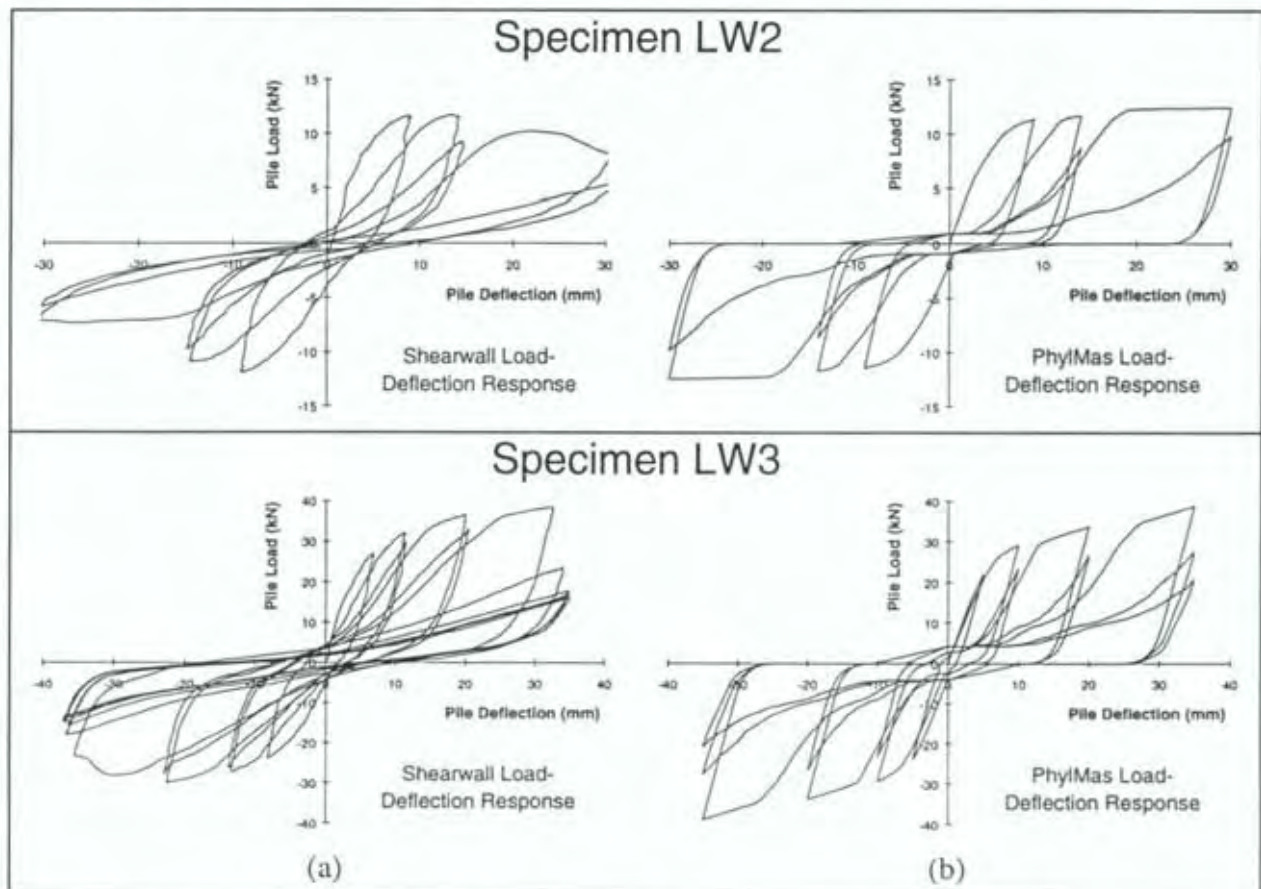


Figure 20 Wall hysteresis loops for: a) Test specimens and b) PhylMas model.

Table 3 PhylMas parameters for long walls.

Parameter	Rk	Ru	Rx	k	Cy	Ry	Jp	Xz	Xp	Xn
Specimen LW2	0.72	1.6	0.4	2.4	11	0.02	1	0.12	0	0
Specimen LW3	0.12	1.3	0.3	5.0	50	.10	1	0.24	0	0

Displacement spectra were generated using PhylMas for the two long wall specimens (Figure 21) using the four earthquakes. An earthquake scale factor of 1.0 and 5 % of critical damping were used to generate the spectra. The mass ratings calculated using Equation 5 with the Figure 21 maximum periods are given in Table 4.

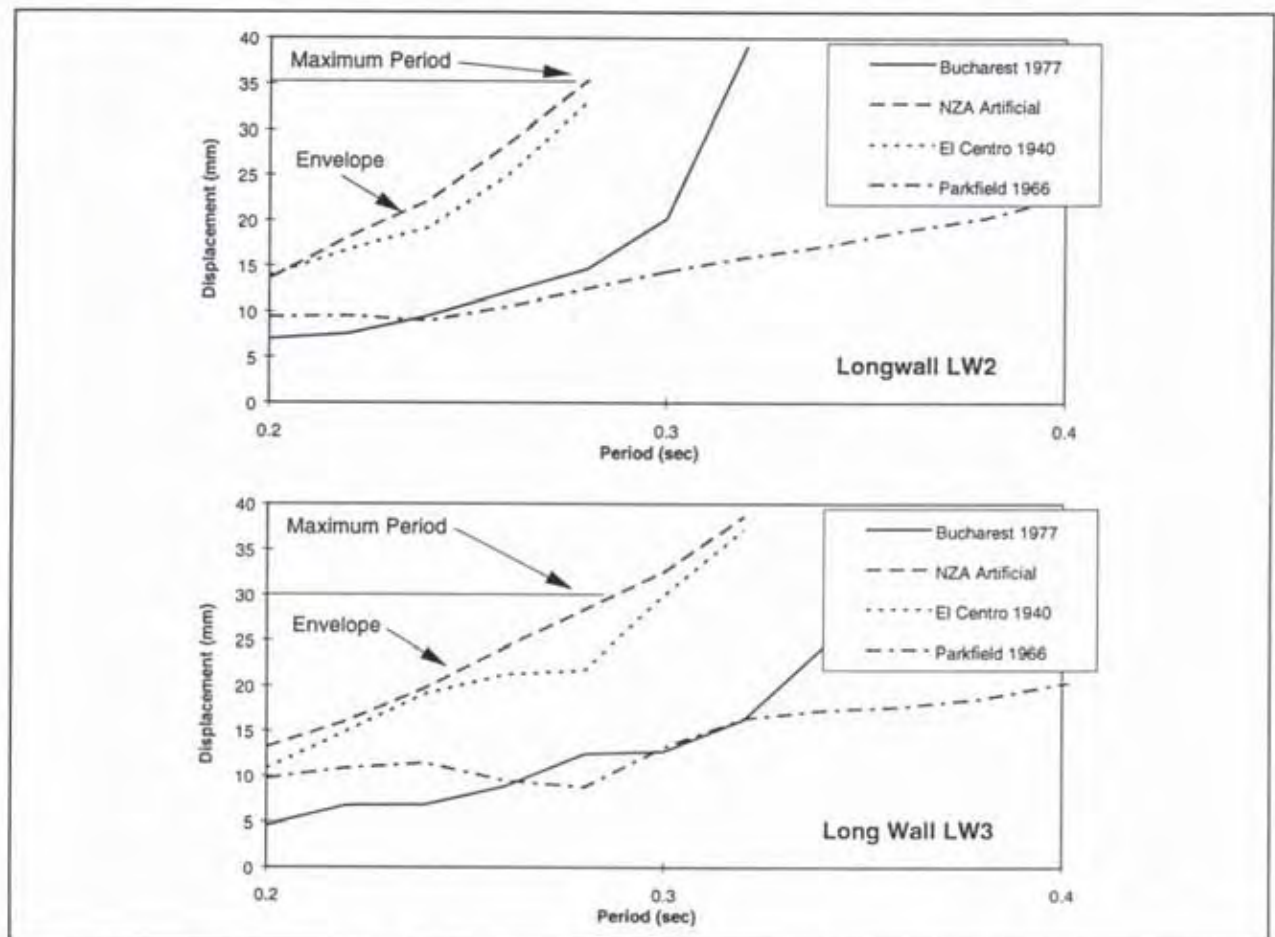


Figure 21 Envelope displacement spectra for long wall specimens.

Table 4 Wall mass ratings from Figure 21 periods.

Wall	Limiting Earthquake	Maximum Test Displacement (mm)	Period T (sec)	Stiffness k (kN/mm)	Mass M (kg)
Long Wall LW2	NZA Artificial	30	0.26	2.4	4100
Long Wall LW3	NZA Artificial	35	0.29	5.0	10600

7.3 Summary

The evaluation method proposed in Section 6 was applied to both relatively flexible pile foundations and to stiff walls. A spreadsheet program was used to plot the displacement spectra and obtain the maximum period and hence calculate the mass able to be restrained by each element.

The stiffer elements (i.e. the two walls and sliding pile B1) were limited by the artificial NZA earthquake, whereas the more flexible elements were limited by the El Centro and Bucharest earthquakes.

8. OVERALL SUMMARY AND CONCLUSIONS

Cantilever poles, moment-resisting frames, diagonal bracing and structural shearwalls are used to resist lateral loads. These bracing elements are required to be stiff to limit structural damage during minor earthquakes but should deform inelastically in a controlled manner during a high-intensity earthquake. The suitability of bracing elements is normally evaluated by racking the elements for a number of cycles in both positive and negative directions.

The load-displacement response plots (hysteresis loops) for the degrading bracing elements typically employed in residential timber buildings are significantly different to those of other structural materials. Five mathematical rules have been proposed by others to model the hysteresis loops of these degrading elements and to simulate the response of the element during an earthquake, using the numerical integration time-history method. A rule developed by Dean (1994), which models a series of springs attached to a rigid bar, was shown to provide the most accurate representation of degrading elements.

A computerised matching system called PhylMas was developed as part of this study to match the bar and spring rule developed by Dean to laboratory test results. This is done by superimposing a plot of the predicted response over a plot of the test specimen response on a computer screen. The predicted response was almost instantaneously updated as the rule parameters were altered, allowing rapid and precise matching.

The PhylMas system was extended to perform non-linear time-history analysis for particular earthquake ground motion records using the simulated element. This used the

bar and spring rule to model the response of a single degree-of-freedom mass and spring oscillator with viscous damping. The natural period of the oscillator was varied by adjusting the mass. A further extension allowed PhylMas to automatically generate displacement and acceleration spectra for a given natural period range. This used a series of time-history analyses, recording the maximum displacement and force for each natural period (or mass).

Good matches were obtained using PhylMas for both quasi-static laboratory racking tests and a plywood wall on a shake table which was subjected to dynamic shaking. Spectral displacements were shown to be most sensitive to the stiffness and degradation properties of the bar and spring rule, whereas spectral accelerations were shown to be most sensitive to stiffness and strength.

A rating procedure was developed for determining the greatest mass able to be restrained by the element for a range of earthquake ground motion records. The procedure utilises displacement spectra generated directly by PhylMas in place of the more commonly used inelastic (ductile) acceleration spectra. This allows the procedure to be applied directly to the element behaviour, avoiding the normal problem associated with degrading systems of having to quantify the yield force in order to assign ductility to the element.

The rating procedure was applied to laboratory test results for a series of relatively flexible piles embedded in the ground and a pair of 4.8 m long by 2.4 m high light timber framed wall specimens to illustrate its application.

PhylMas and the bar and spring rule have been shown to provide a reliable method of rating the mass able to be laterally restrained by degrading structural elements. This allows degrading elements to be used with confidence and avoids assigning pseudo yield and ductility to elements without a natural yield limit.

9. RECOMMENDATIONS FOR FURTHER RESEARCH

1. PhylMas should be verified against a greater range of experimental results. This includes both static elements subjected to asymmetric cyclic loading (i.e. more representative of earthquake motion) and shake table tests.
2. PhylMas is currently only able to analyse one single-degree-of-freedom element but should be extended in order to analyse:
 - a) several elements subjected to the same displacement. This is required to examine the behaviour of typical construction practice where elements with high stiffness resist load in parallel with elements having lower stiffness (e.g. short and tall piles or glued plasterboard walls with plywood shearwalls);
 - b) a heavy roof restrained by shearwalls founded on flexible piles; and
 - c) several elements attached to a rigid body which is able to translate and rotate. (e.g. a complete pile foundation system beneath a rigid floor diaphragm.)

3. Earthquake spectra for some foundation piles suggest that a nominal ductility could be assigned to an element. This should be explored further for a range of element types as this could allow ductility and yield values to be assigned to elements for use with the normal code-based acceleration spectra design methods.

10. REFERENCES

- Buchanan, A.H. 1989. Bracing and Diaphragms. *In* Timber Use Manual, Section B-3, Buchanan, A.H. (Ed.), New Zealand Timber Industry Federation (Inc.), Wellington.
- Carr, A.J. and Moss, P.J. 1994. Impact Between Buildings During Earthquakes. *Bulletin, New Zealand National Society for Earthquake Engineering* 27(2): 107-113.
- Clough, R.W. and Penzien, J. 1975. *Dynamics of Structures*. McGraw-Hill. New York.
- Cooney, R.C. and Collins, M.J. 1979 (revised 1982, 1987, 1988). A wall bracing test and evaluation procedure. Building Research Association of New Zealand Technical Paper P21. Judgeford.
- Dean, J.A., Stewart, W.G. and Carr, A.J. 1986. The Seismic Behaviour of Plywood Sheathed Shearwalls. *Bulletin, New Zealand National Society for Earthquake Engineering* 19(1): 48-63.
- Dean, J.A., Stewart, W.G. and Carr, A.J. 1987. The Seismic Design of Plywood Sheathed Timber Frame Shearwalls. *Pacific Conference on Earthquake Engineering, Wairakei, New Zealand*. 2:165-175.
- Dean, J.A. 1994. Personal communication.
- Dolan, J.D. 1991. A Numerical Model to Predict the Dynamic Response of Timber Shear Walls. *Proceedings, International Timber Engineering Conference, London*. 4: 338-345.
- Dowrick, D.J. 1977. *Earthquake Resistant Design*. John Wiley & Sons, Chichester.
- MacRae, G.A. 1989. The Seismic Response of Steel Frames. PhD Thesis, Dept. of Civil Eng. University of Canterbury.
- Norton, J.A., King, A.B., Bull, D.K., Chapman, H.E., McVerry, G.H., Larkin, T.J. and Spring, K.C. 1994. Northridge Earthquake Reconnaissance Report. *Bulletin, New Zealand National Society for Earthquake Engineering* 27(4): 235-344.
- Park, R. 1989. Evaluation of Ductility of Structures and Structural Assemblages from Laboratory Testing. *Bulletin, New Zealand National Society for Earthquake Engineering* 22(3): 155-166.
- Reardon, G.F. 1980. Recommendations for the Testing of Roofs and Walls to Resist High Wind Forces, Technical Report No. 5, Cyclone Testing Station, James Cook University, Queensland.

- Standards Association of New Zealand. 1990. Code of Practice for Light Timber Frame Buildings not Requiring Specific Design. NZS 3604. Wellington.
- Standards New Zealand. 1992. General Structural Design and Design Loadings for Buildings. NZS 4203. Wellington.
- Standards New Zealand. 1993. Timber Structures Standard. NZS 3603. Wellington.
- Shephard, R.B., Wood, P.R., Berrill, J.B., Gillon, N.R., North, P.J., Perry, A.K. and Bent, D.P. 1990. The Loma Prieta, California, Earthquake of October 17, 1989: Report of the NZNSEE Reconnaissance Team, Bulletin, New Zealand National Society for Earthquake Engineering 23(1): 1-78.
- Stewart, W.G. 1987. The Seismic Design of Plywood Sheathed Shearwalls. Thesis submitted in partial fulfilment of PhD Degree, University of Canterbury, Christchurch, New Zealand.
- Thurston, S.J. 1994. Field Testing of House Pile Foundations Under Lateral Loading. Building Research Association of New Zealand. Study Report SR58. Judgeford.

APPENDIX A: USER MANUAL FOR PHYLNAS PROGRAM

This appendix describes the how to install the PhylMas program and use it to match pinched hysteresis loops from pseudo-static reverse-cyclic test specimens.

A1. Installing PhylMas

The program requires an IBM-compatible personal computer with Microsoft Windows (version 3.1 or later). The computer does not require a co-processor (i.e. a 386+387 or a 486DX) but a co-processor significantly decreases the time required to perform time-history analyses. It is assumed that the user has some familiarity with Windows software. The current version requires Windows to use a 'VGA resolution' (640x480) colour monitor as it cannot adapt to higher resolution (eg SVGA) monitors.

Use the Setup program (SETUP.EXE) to set up PhylMas as follows:

1. Insert the installation disk into the disk drive.
2. Start Windows.
3. From the Windows Program Manager, select 'Run' from the 'File' menu and Windows will display the Run dialog box.
4. Type **a:setup** in the Command Line box.
5. Choose the 'OK' button.
6. Follow the setup instructions on the screen. After a while the setup program will ask where the PhylMas program is to be installed. The default and recommended location is directory **c:\phylmas** on the **c:** drive. Clicking on the 'Continue' button will copy the program files to the chosen location. Some additional files will be copied to the Windows 'system' directory but this should not concern the user (unless there is not enough free space on the hard disk).

After installing the program, the Setup program creates a PhylMas program group and places the PhylMas icon in the group.

The program is then run by double-clicking the PhylMas icon in the Windows Program Manager.

The earthquake library only has seven records as most users will already have their own library. The method of configuring PhylMas to use other earthquake record libraries is described later. PhylMas will also have to be reconfigured if it is not installed in the **c:\phylmas** directory as described in step 6 above.

A2. Program Description

A2.1. Program Screen

The program has a main window, similar to that shown in Figure A1, containing a hysteretic plot and the generating parameters (described in Section 2.2) required to match a hysteretic plot. Each parameter has a box in the lower third of the window that displays the current value (which may be changed by clicking on it). Alternatively, the parameter may be changed by clicking on the square in the "slider bar" and moving it to the left (decreasing the parameter) or right (increasing it). The hysteretic plot is initially blank and is generated by clicking the 'Recalc' button. This allows several parameters to be modified before the new plot is generated. Hysteretic, Displacement or Force plots can be displayed by clicking on the appropriate 'Tab' above the graph.

The mouse pointer changes as it moves around the screen. It changes to a cross-hair when over the graph (displaying the current ordinates at the bottom of the screen), and displays a brief description of each variable at the bottom of the screen when over the value.

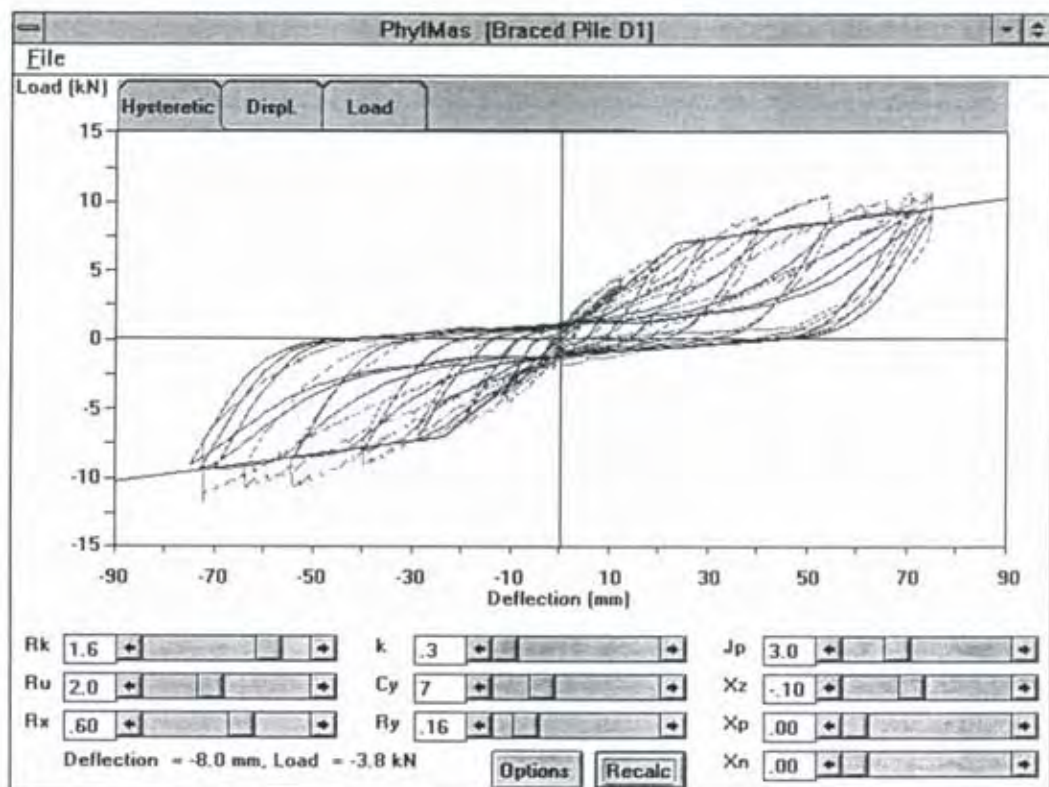


Figure A1 PhylMas program screen.

A2.2. Analysis Controls

The operation of the program is changed by clicking the 'Options' button that displays the Analysis Controls dialog box (Figure A2(a)). The initially selected 'Static' Analysis Type (selected in the upper left of the Figure A2(a) dialog box) defines the displacement cycles¹ applied to the test specimen. A mini-spreadsheet in the dialogue box has two columns; the first defines the number of cycles at the displacement-specified in the second. Both cells below the last pair of values are required to be empty. The displacement increments used to generate the plot and the title of the plot are specified below the spreadsheet. 'Plot Yieldlines' allow the Figure 4(b) bi-linear envelope to be superimposed on the hysteretic plot (plotted with a blue line). The dialogue box is closed by clicking the Close button.

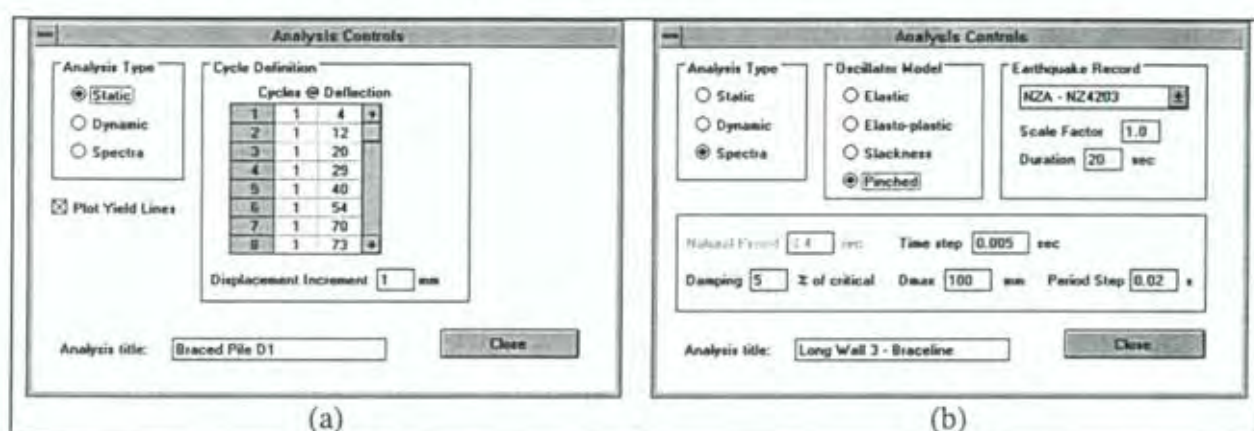


Figure A2 Analysis controls for: a) 'Static' cycle definition and b) 'Dynamic' time-history analysis.

The Dynamic and Spectra Analysis Types change the Analysis Controls dialog box as shown in Figure A2(b). The oscillator model, earthquake record and other parameters for the time-history analysis are changed from this dialog box. The default oscillator model is elastic. The oscillator models (Figure 3) have different numbers of 'generating parameters' so the parameters not applicable to a particular model are disabled (and coloured grey) on the main screen when that oscillator is selected (e.g. only k is required for the elastic oscillator model).

The earthquake record is selected from the record library by clicking the ↓ and then the required record name. The scale factor is applied to the acceleration for each time-step in the earthquake record. The duration of the record is initially set to the length of the chosen record but may be reduced.

The Natural Period (T), Time step and Damping are required for the time-history analysis. The maximum deflection, D_{max} , and period step are not

¹ One cycle constitutes displacement in the positive direction to the specified deflection, displacement to a negative deflection of the same magnitude, finally returning to the zero deflection.

required for the Dynamic analysis and are disabled. It is enabled for the Spectra analysis but the Natural Period is disabled because it is automatically generated.

A2.3. Menus

The 'File' menu has six functions:

Open Param allows the generating parameters and cycle definition data from a previous analysis to be recalled. Selecting this item produces a standard Windows File dialog box and the user selects a previously saved configuration file from disk. The data is stored in a file with a '.lad' suffix.

Save Param allows the generating parameters and cycle definition data to be saved for future recall. Selecting this item produces a standard Windows File dialog box and prompts the user for a configuration file name. The data is stored in a file with a '.lad' suffix that is automatically added by the program.

Load Loop specifies a file containing the hysteretic loops from the reverse-cyclic pseudo-static test that is being matched. Selecting this item produces a standard Windows File dialog box and the user selects a hysteretic loop data file from disk. These are plotted on the screen and the generated loops are plotted on top of them. The file is not required for the program to operate but it simplifies the comparison of the two. The data is required to have two columns within a normal text file (i.e. not a spreadsheet or word processor file) with displacement (mm) in the first column and load (kN) in the second. (The columns must be separated by space characters at present - Tab characters are not correctly interpreted by Visual Basic)

Save Data saves the data generated by the program in a disk file. Selecting this item produces a standard Windows File dialog box and prompts the user for a data file name. This file contains two columns (displacement in mm and force in kN) for 'Cyclic' analysis; three columns (time in sec, displacement and force) for 'Dynamic' analysis; and three columns (period in sec, spectral displacement in mm and spectral acceleration in g) for 'Spectra' analysis.

Exit quits the program and returns to Windows. If any of the generating parameters were changed the user is asked whether they should be saved before quitting.

The four most recently used data definition files may be recalled by selecting their name from the bottom of the File menu. The program automatically loads the most recently used file when started up.

A3. Modelling the Experimental Data

The following procedure is used to model experimental data with a plot of the load-displacement hysteretic plot and the PhylMas program. Use Figure 4 as an indication of the effects of the generating parameters; the plot produced

will be a 'smoothed' combination of the bi-linear (Figure 4(b)) and slack (Figure 4(c)) spring components. It should be noted that it will be an iterative process, because changes in most of the parameters affect others, so the initial estimates only have to be approximate.

1. Click the 'Options' button. Select the 'Static' analysis type and enter the number of cycles and the target displacements (in mm) used during the test. Then enter the displacement increment (1 mm will usually be small enough although it may need to be reduced further if the maximum displacement was less than 20 mm), the title, and click the Close button.
2. If the test record is stored in a disk file, load this using the Load Loop option from the File menu.
3. Estimate the initial stiffness k (in kN/mm) from the test hysteretic plot. Set the k parameter to about 90 % of this value as described above.
4. Estimate the Figure 4 yield force, f_y , entered as parameter C_y (in kN), and the slope of the bi-linear line, entered as the ratio R_y .
5. Estimate the reloading stiffness and unloading stiffness ratios R_k and R_u from the hysteretic plot in a similar manner and enter them as R_k and R_u respectively.
6. Estimate the J_p ("pinch") parameter that controls the number of separated to non-separated springs. A small value produces very pinched loops (with a small load at zero deflection) and a large number makes the loops "fatter". A value of 5 is a suitable initial estimate unless the hysteretic loops are particularly pinched.
7. Estimate the R_x parameter (from the displacement where the load passes through zero).
8. Enter values of 0 (zero) for X_z , X_p , and X_n respectively (these are described below).
9. Generate a plot using the current parameters by clicking the 'Recalc' button. After a time (depending on how large the displacement increment is and how fast the PC is) a plot will be produced on the screen.
10. Change the parameters until the plot is reasonably similar to the experimental plot. The X_z parameter may now be adjusted. Increasing a positive value of X_z increases the degradation of the second and subsequent cycles to each displacement level, with a value of 0.1 causing a significant reduction in some cases. Decreasing a negative value of the X_z parameter 'fattens' the loops at small displacements before yield occurs. The X_n parameter specifies the amount of slackness initially present in the system, and would not normally be more than 10 mm.

A4. Setting up the Earthquake Record Library

The earthquake library is supplied with seven earthquake records, as described above. Additional records are added to the program by editing a configuration file which contains details of each of the earthquake records and where they are stored.

The configuration file is called PHYLMA.INI and is stored in the Windows directory (usually C:\WINDOWS). It should only be changed with a text editor (or saved as a text file if edited with a word processor) or PhylMas will not be able to read it. The original contents of the file are as follows:

```
[Quake Records]
NumQuakes=7
Quake1=NZA - NZ4203,20,c:\phylmas\eqdatb.dat
Quake2=2 x NZA,40,c:\phylmas\eqdat2.dat
Quake3=E1 Centro 1940,20,c:\phylmas\eqelc.dat
Quake4=Parkfield 1966,30,c:\phylmas\parkf3.dat
Quake5=Pacoima 1971,40,c:\phylmas\pacom3.dat
Quake6=Bucharest 1977,16,c:\phylmas\buchnsc.eqd
Quake7=SC89 Soft,38,c:\phylmas\eqdatsc.dat

[Recent Files]
File1=pd1.lad
File2=pj4.lad
File3=pb1.lad
```

The earthquake data is at the top of the file in the section headed [Quake Records]. The first line contains the number of earthquake records that follow it; in this example it is set to 7. Subsequent lines (with Quake1=, Quake2=, ... at the start) define each earthquake record. The data after the equals sign (=) contains three parts separated by commas (,):

1. The label that appears in the Analysis Controls dialog box (and may include space characters);
2. The approximate duration of the record in seconds; and
3. The full name of the earthquake record file, including the path. This allows earthquake records to be stored in different directories.

The earthquake record file is restricted to two 'custom' formats at present (to simplify the program, but will be altered to read standard Caltech and Berg formats soon):

1. A file (with a '.dat' suffix) containing a title on the first line; the number of time-acceleration data pairs on the second line; and 1 to 4 time-acceleration data pairs with elapsed time in sec and accelerations in g on the remaining lines. e.g.

```
STAR ARTIFICIAL NEW ZEALAND-A, NZ4203A, BERG FORMAT
990
0.0000 -0.002550 0.0200 -0.002550 0.0400 -0.002550 0.0600 -0.001700
0.0800 -0.002550 0.1000 -0.003400 0.1200 -0.012750 0.1400 -0.015300
```

2. A file (with a '.eqd' suffix) containing a title on the first line; the number of acceleration values, the time increment, the scale factor applied to the accelerations to convert them to mm/sec/sec, the initial displacement (in mm) and the initial velocity (in mm/sec) the on the second line; and any number of accelerations on each of the remaining lines, e.g:

```
Bucharest Mar 77 N-S
810 0.020 9810.0 0.0 0.0
-0.005739 -0.012130 -0.007574 -0.002875 -0.000601 0.001009 0.001835 0.003150
```

A5. Source Code

The source code for PhylMas is located in the \SRC subdirectory of the distribution disk. The files in that directory are as follows:

main.frm	This defines the default screen - control sliders etc.
ctrl.frm	Defines the 'control panel' for earthquakes and hysteresis loops.
module1.bas	This contains the dynamic analysis and other support code.
files.bas	Deals with reading and writing files on disk.
hyst.dat	Definitions for bi-linear and separated springs (read by module1).
PhylMas.mak	Visual Basic Make file.
PhylMas.vbz	File for creating the distribution disk (Visual Basic Pro).
main.frx	A second copy of the program icon.
PhylMas.ico	Icon for the program.
*.bmp	Bitmaps for tabs which change the plot type on the graph.
main.frx	A supplement to main.frm - contains bitmaps.

APPENDIX B: LONG WALL ASSESSMENT PROGRAMME

A number of lateral load-resisting shearwalls lined with degrading sheet materials (such as paper faced gypsum board) were severely overloaded and collapsed during the Northridge, Los Angeles, earthquake of 17 January 1994 (Norton et al., 1994). This had not been apparent in earlier testing of shearwall systems in New Zealand. For the research reported here, four walls with similar geometry to those damaged were built, loaded with gravity loads representative of three storeys supported by the wall and tested under lateral load.

The four wall test specimens were 4.8 m long and 2.4 m high, with studs spaced at 600 mm centres and plasterboard attached to one face of the timber framing (Figure B1). The framing was assembled using 100 × 4.0 mm framing nails. The plasterboard was attached to the framing as shown in Figure B1 and summarised in Table B1 for the four specimens. Joints between the plasterboard sheets were filled and reinforced according to the plasterboard manufacturer's instructions. Specific construction details are given in the following sections for each specimen.

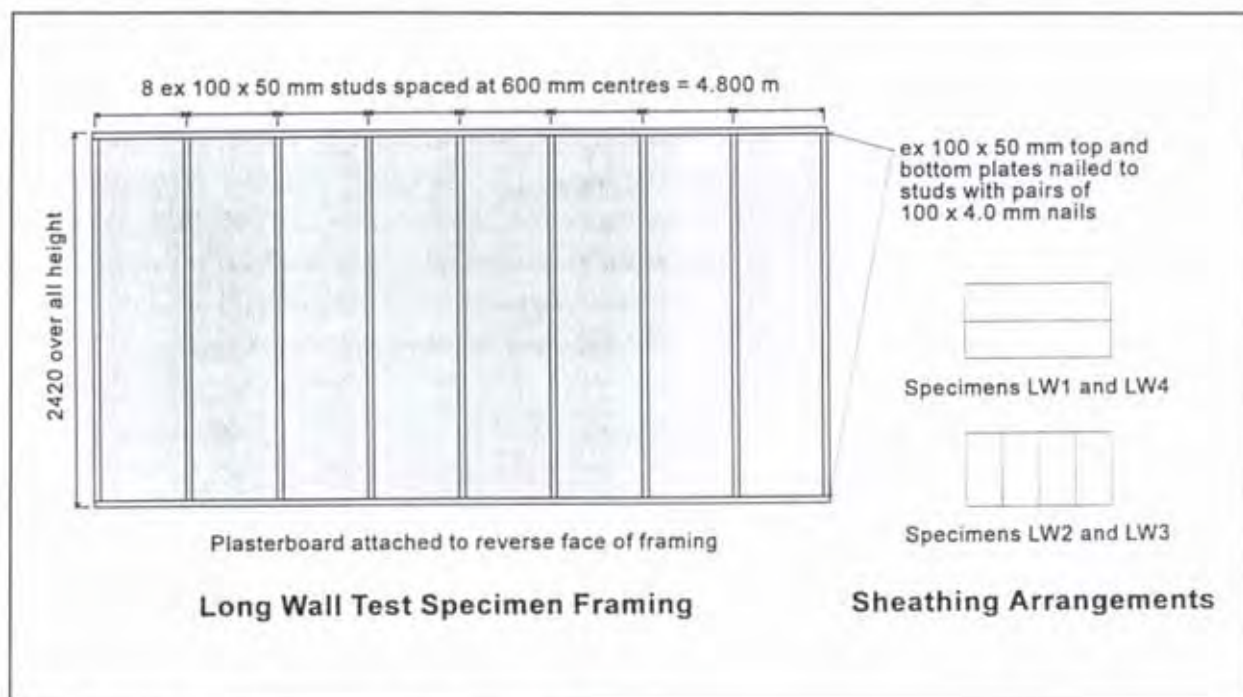


Figure B1 Long wall specimen details.

Table B1 Shearwall Test Specimen Detail Summary.

Specimen Label	Plasterboard Sheet			Fasteners
	Type	Dimensions	Orientation	
LW1	Type A	4.8 × 1.2 m	Horizontal	30×2.5 mm flat head nails and glue at intermediate studs
LW2	Type B	1.2 × 2.4 m	Vertical	30×2.5 mm flat head nails
LW3	Type B	1.2 × 2.4 m	Vertical	30×2.5 mm flat head nails with 15 mm dia. steelwashers
LW4	Type A	4.8 × 1.2 m	Horizontal	30×2.5 mm flat head nails and glue at intermediate studs

The specimens were sequentially attached to the foundation beam, instrumented and tested. They were nailed through particle board flooring to a timber foundation beam as shown in Figure B1. The specimens were racked horizontally using a displacement-controlled hydraulic actuator attached (via a steel channel) to the left end of the top framing plate, as shown in Figure B2 and Figure B4. A system of levers and weights was used to apply a total gravity load of 1750 kg along the length of the specimen. This was uniformly distributed between 6 of the 9 studs. Pairs of rollers were mounted either side of the specimen (Figure B4(b)) to minimise out-of-plane movement of the top framing plate.

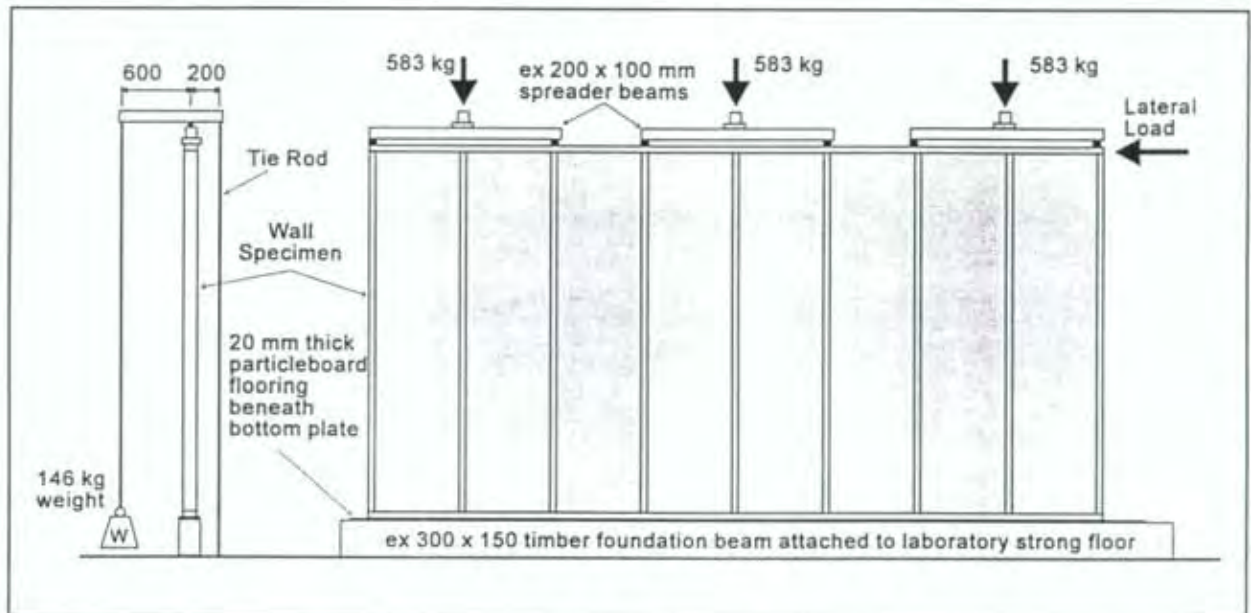


Figure B2 Test arrangement for long wall specimens.

Displacements were measured with linear potentiometers at the locations indicated in Figure B3. These measured the lateral displacement of the top and bottom framing plates and the movement of the plasterboard relative to the framing plates and end studs. The applied load was measured with a load cell in series with the hydraulic actuator. Loads and displacements were recorded continuously with a PC based data acquisition system whenever the actuator was being operated. Extension of the actuator was taken as the positive direction, and retraction as the negative.

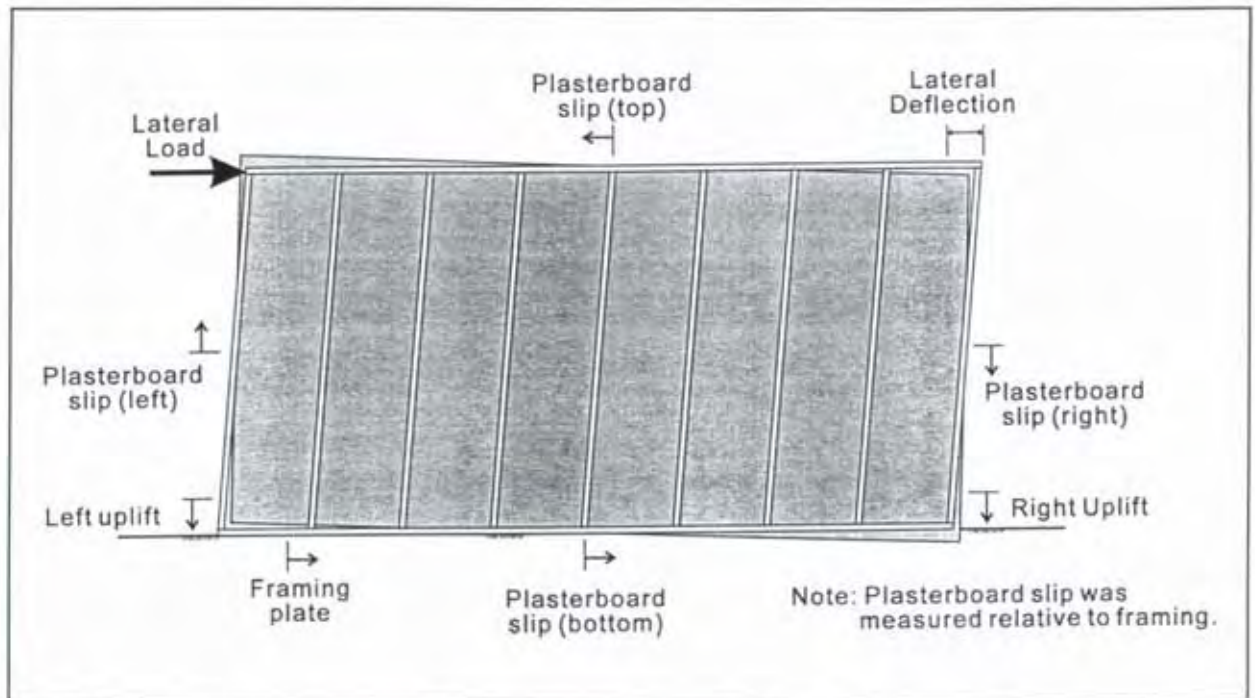


Figure B3 Displacement measurement positions for the shearwall specimens.



Figure B4 Test arrangement for long wall specimens: a) Viewed from the framing face and b) Viewed from the plasterboard face.

B1. Specimen Deformation

Four modes of deformation were observed in the shearwall specimens. These are illustrated separately in Figure B5, although the specimens had a combination of deformation modes.

Specimens LW1 and LW4 (glued and nailed) deformed mostly in mode III because the sheathing was glued to the studs and hence restrained from rotating (i.e. mode II deformation). Mode IV was only observed during the first cycle when the load was greatest. Mode I was neither measured nor observed but tests by Thurston (1994) indicate that this would only contribute a deflection of 1 mm for 20 kN applied load.

Specimens LW2 and LW3 (nailed only) deformed in mode II at low loads, but changed to mode III toward the end of the test. The centre vertical plasterboard joint ruptured in Specimen LW3 and the greatest nailslip occurred along the bottom framing plate (i.e. mode III) with the left half of the plasterboard, and along the centre stud with the other half. Specimen LW3 showed significant mode IV deformation prior to rupturing when the vertical load applied to the left stud by the sheathing fasteners was greater than the vertical gravity load.

	<p>I) Shear deformation: The lateral deflection arises from shear deformations within the sheathing material. The lateral deflection at the top of the framing is the same as that of the sheathing.</p>
	<p>II) Perimeter nailslip: The sheathing material rotates as a rigid body due to nailslip around the perimeter framing (from shear transfer between the sheathing and framing). The framing deformation is the same as that for shear deformation.</p>
	<p>III) Nailslip along one edge: The sheathing remains attached to three of the four perimeter framing members. Nailslip along the fourth member (the bottom framing plate in this figure) causes curvature of the perpendicular framing (studs).</p>
	<p>IV) Rigid body rotation: The wall lifts at one end, rotating as a rigid body about the corner at the opposite end.</p>

Figure B5 Shearwall deformation modes.

Static analysis of the shearwall specimens showed that the vertical gravity loads would increase the lateral load applied to the specimen, possibly to the point of instability, when the displacement was greater than the stud width. The predicted additional force is plotted against the displacement of the top

plate in Figure B6 which also shows that the gravity load provides a (negative) restoring force for displacements smaller than the stud width.

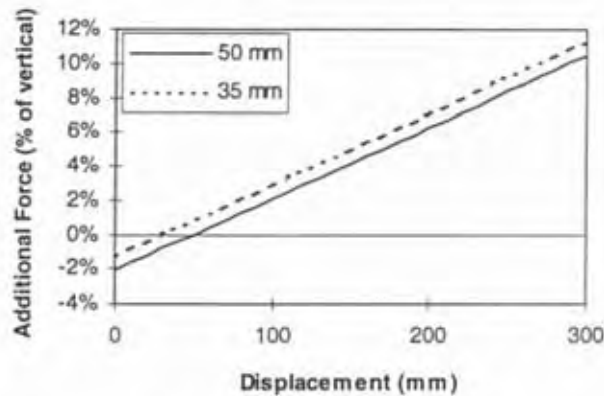


Figure B6 Additional lateral force from gravity load for 50 and 35 mm stud widths.

As an example, at 100 mm displacement the additional force from the 1750 kg gravity load was predicted to be 0.43 kN for the 50 mm wide studs and 0.57 kN for the 35 mm wide studs. The test specimens did not become unstable because the additional forces were lower than the residual specimen strength (at the maximum displacements the specimens were subjected to). Further, the lateral movement of the loading mechanism would have induced restraining loads of a similar magnitude in some instances.

B2. Specimen LW1

B2.1. Specimen LW1 Construction

Specimen LW1, intended to be representative of construction normally used in Australia and the U.S., was clad with two 4.8 m long by 1.2 m high sheets of Type A plasterboard as shown in Figure B1. The framing was ex 100 x 50 mm radiata pine. The plasterboard was attached to the framing around the perimeter with 30 x 2.5 mm flat head galvanised nails spaced at 150 mm centres and glued to the intermediate studs with approximately 50 x 50 mm glue patches at approximately 240 mm centres.

B2.2. Specimen LW1 Schedule

The test schedule for Specimen LW1 is given in Table B2. This gives the target deflection at each cycle peak along with the measured deflections and loads.

The specimen was racked with one ± 10 mm cycle followed by two ± 30 mm cycles and two ± 90 mm cycles. The actuator was set to apply the full (i.e. positive and negative) loading cycle over a period of 10 seconds.

Table B2 Specimen LW1 Test Schedule.

Cycle	Target Lateral Deflection (mm)	Lateral Deflection (mm)	Measured		
			Lateral Load (kN)	Left Uplift (mm)	Right Uplift (mm)
+1	10	8.0	19.1	2.0	-2.3
-1	-10	-8.4	-17.9	-1.9	1.7
+2	30	30.8	16.0	2.2	-2.4
-2	-30	-31.3	-4.4	1.3	1.2
+3	30	31.3	3.0	1.6	0.5
-3	-30	-31.3	-3.1	0.9	1.3
+4	30	31.3	2.8	1.6	0.5
-4	-30	-31.6	-3.1	1.0	1.3
+5	90	94.1	3.6	1.6	0.4
-5	-90	-89.1	-1.8	0.8	1.3
+6	90	94.5	0.5	-	-
-6	-90	-92.9	-0.9	-	-



Figure B7 Deformed shape of framing at +30 mm top plate lateral displacement.

B2.3. Specimen LW1 Description

**Cycle 1
±10 mm** There was minor degradation of the plasterboard around the nails attaching it to the bottom framing plate during this cycle. The remaining plasterboard nails and glue appeared to be undamaged.

**Cycles 2 to 4
±30 mm** The nails along the bottom framing plate failed in mode III (Figure B5) by pulling completely through the plasterboard during the first cycle to +30 mm. Nails at the actuator end pulled through first, followed almost immediately by a progressive shear failure along the remainder of the bottom plate. Failure of the plasterboard nails along the bottom plate was followed by failure of both nailed and glued connections between the lower plasterboard sheet and the studs. There appeared to be little damage to the nails or glue attaching the upper plasterboard sheet to the framing. Thus the lower half of each stud curved because it remained attached to both the upper half of the plasterboard and the bottom plate, as shown in Figure B7.

Figure B7 also shows the plasterboard separating from the framing as the nails were pulled through the vertical edge of the sheet. The plasterboard was separated from the bottom plate after the nails had pulled through the plasterboard, as shown in Figure B8. This also subjected the glue to both tensile and shear loads, causing the paper facing to be torn off the plasterboard around the glued regions.

There appeared to be little further damage as the remainder of cycle 2 or cycles 3 and 4 were applied.

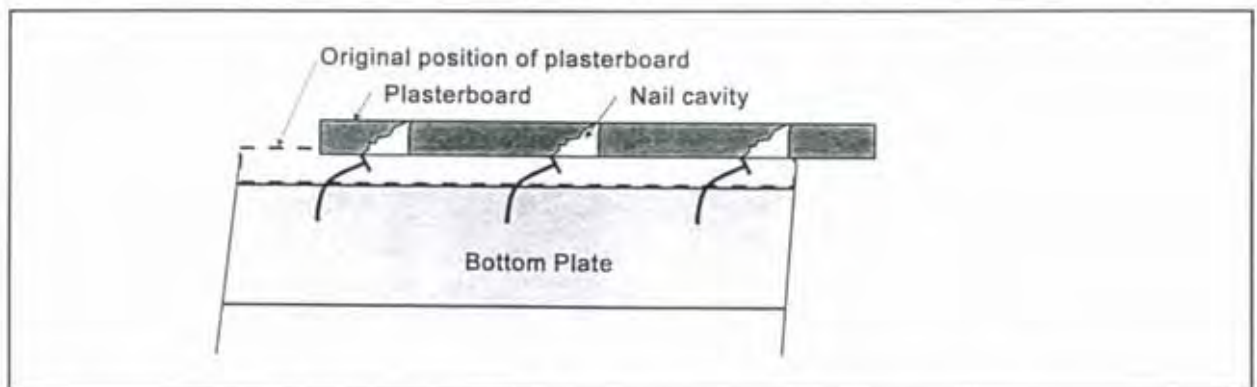


Figure B8 Sectional plan view of wall base showing plasterboard separating from bottom plate.

**Cycles 5 to 6
±90 mm** The upper plasterboard sheet separated from the studs during cycle +5 as the glue and nails failed as described above but it remained attached to the top framing plate. There was no further damage during the remainder of cycle -5 or during cycle 6.

The framing face of the lower sheet of plasterboard, which was completely detached from the top plate after cycle 6, is shown in Figure B9. This shows the regions where the glue pulled the paper face from the board and where the bottom framing plate nails pulled through and scarred the surface.



Figure B9 Framing face of plasterboard after test.

B2.4. Specimen LW1 Results

The load-displacement response of Specimen LW1 is given in Figure B10. The maximum load of 19.1 kN occurred during cycle +1 (at +8 mm). The load at +8 mm during cycle 2 was half of the maximum load, rising to 80% of the cycle 1 load before failure of the plasterboard nails. The load was considerably lower at ± 30 mm, where the sheathing had detached from the bottom plate, and almost negligible at ± 90 mm when the sheathing was no longer attached to any of the studs.

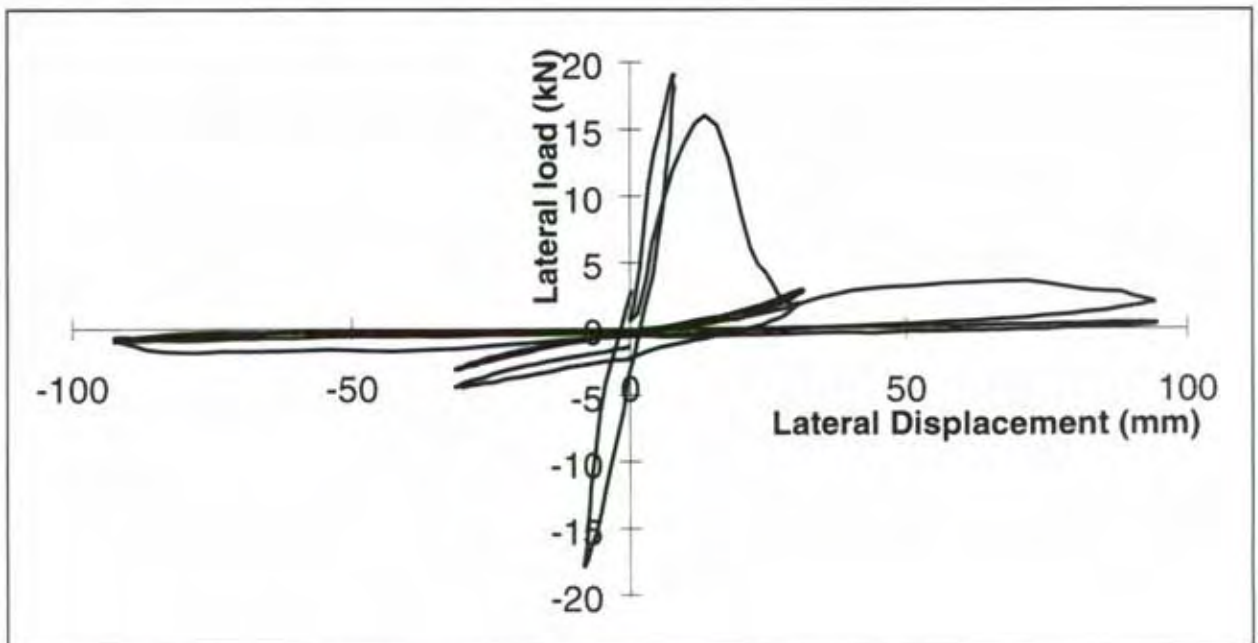


Figure B10 Load-displacement response of Specimen LW1.

Nailslip between the plasterboard and the perimeter framing members (measured close to the centre of and along the axis of the framing member) is given in Table B3.

Table B3. Perimeter Plasterboard Nailslip for Specimen LW1.

Cycle	Lateral		Plasterboard			
	Deflection (mm)	Load (kN)	Top (mm)	Bottom (mm)	Left (mm)	Right (mm)
+1	8.0	19.1	1.7	-3.0	2.3	-0.3
-1	-8.4	-17.9	-1.7	3.0	-1.7	0.3
+2	30.8	16.0	2.2	<-25	2.4	-0.4
-2	-31.3	-4.4	1.0	> 25	-1.2	1.0
+3	31.3	3.0	0.8	-	-0.5	0.4
-3	-31.3	-3.1	0.4	-	-1.3	1.2
+4	31.3	2.8	0.8	-	-0.5	0.4
-4	-31.6	-3.1	0.4	-	-1.3	1.2
+5	94.1	3.6	1.1	-	-0.5	-
-5	-89.1	-1.8	0.3	-	-1.3	-
+6	94.5	0.5	-	-	-	-
-6	-92.9	-0.9	-	-	-	-

B3. Specimen LW2

B3.1. Specimen LW2 Construction

Specimen LW2, intended to be representative of wall construction normally used in New Zealand, had four 1.2 m long by 2.4 m high (i.e. vertical) Type A plasterboard sheets attached to ex 100 x 50 mm framing, as shown in Figure B11. The plasterboard was attached to the framing with 30 x 2.5 mm nails spaced at 300 mm centres around the perimeter of each sheet and to the intermediate studs with pairs of the same nails spaced at 300 mm centres. (The plasterboard was attached to the opposite face of the framing used for Specimen LW1.)



Figure B11 Construction details for Specimen LW2.

B3.2. Specimen LW2 Schedule

The test schedule for Specimen LW2 is given in Table B4.

Table B4 Specimen LW2 Test Schedule.

Cycle	Target Lateral Deflection (mm)	Measured			
		Lateral Deflection (mm)	Lateral Load (kN)	Left Uplift† (mm)	Right Uplift† (mm)
+1	10	9.0	11.7	1.4	-1.2
-1	-10	-9.2	-11.8	-0.7	0.9
+2	15	14.2	11.8	1.6	-1.6
-2	-15	-14.6	-10.9	-0.8	1.0
+3	15	14.6	9.3	1.2	-1.4
-3	-15	-15.0	-9.7	-0.7	0.9
+4	30	21.8/ 30.6	10.3/ 8.2	1.8	-2.3
-4	-30	-30.6	-7.0	-1.4	1.5
+5	30	31.0	5.4	1.5	-2.2
-5	-30	-31.0	-6.1	-1.3	1.3
+6	60	62.6	4.5	2.1	-3.2
-6	-60	-62.1	-4.5	-2.0	2.4
+7	60	62.8	3.2	1.8	-3.1
-7	-60	-62.4	-3.7	-2.0	1.8
+8	60	62.9	2.8	1.8	-3.0
-8	-60	-62.1	-3.5	-1.9	1.7
+9	60	62.9	2.7	1.8	-3.1
-9	-60	-62.4	-3.5	-2.0	1.7

† Uplift measurements were magnified by 10 to 20 % because the potentiometers were away from the centre line of the stud.

B3.3. Specimen LW2 Description

Cycle 1 There was some deformation of the plasterboard around the nails in the
±10 mm bottom framing plate but no other visible damage.

Cycles 2 to 3 There was a significant amount of plasterboard deformation around the nails
±15 mm in the top and bottom plates and the lower regions of the end studs. The
 greatest deformation around was around the nails in the bottom plate and a 20
 × 30 mm piece of plasterboard broke away adjacent to a corner nail. There
 was also some deformation around the plasterboard nails in the lower regions
 of the intermediate studs.

Cycles 4 to 5 All of the nails in the end studs pulled through the edges of the sheets of
±30 mm plasterboard. The lower two pairs of nails in the studs without sheet joints also
 showed signs of plasterboard deterioration. There appeared to be no further
 damage around nails in the upper half of the specimen.

Cycles 6 to 9 The damage in these cycles was similar to but more extensive than that of
 ± 60 mm cycles 4 and 5. Figure B12 shows the curvature developed in the lower regions of the studs during the positive part of cycle 6.

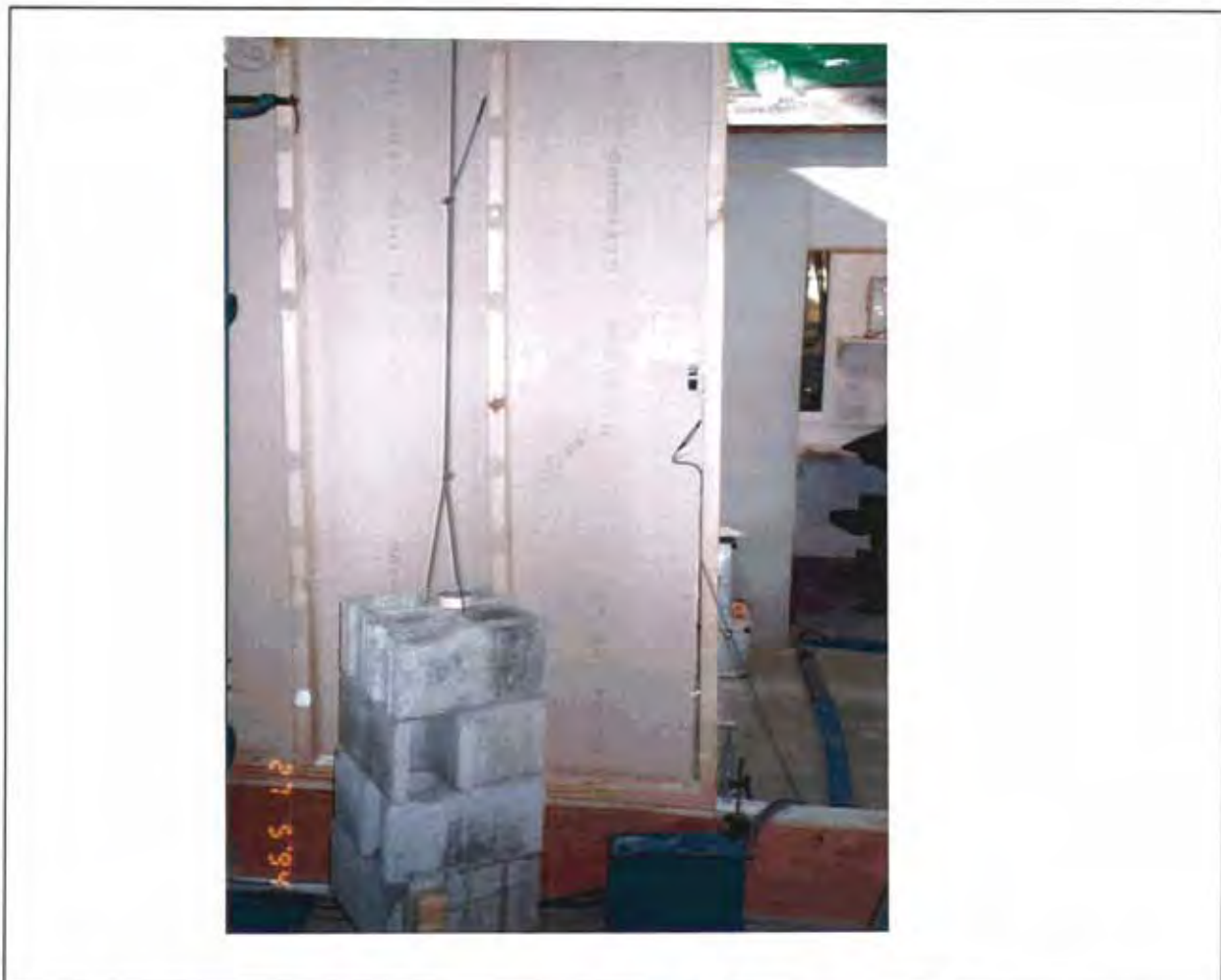


Figure B12 Stud curvature in Specimen LW2 at a +60 mm displacement.

Push to Failure

All of the deflection potentiometers except the one measuring lateral deflection were removed to avoid damage, and the specimen was racked to +290 mm. The nails attaching the plasterboard to the studs were progressively pulled through the plasterboard until the whole stud was free. This is illustrated in Figure B13, which shows the specimen at the end of the test with some studs still attached to the top of the plasterboard and developing significant curvature. The studs directly beneath the vertical load application points appeared to remain attached longer than the others, possibly because the axial load itself was contributing to the curvature.



Figure B13 Specimen LW2 at the end of the test (+290 mm displacement).

B3.4. Specimen LW2 Results

The load-displacement responses of Specimen LW2 are given in Figure B14. This specimen sustained much greater displacements than Specimen LW1. (A complete comparison of the specimens is given at the end of the individual specimen descriptions.) The load reduced almost linearly with displacement from 70 to 200 mm during the push to failure (Figure B14(b)) and then began to increase again. The load decrease indicates instability developing from the presence of the gravity load, which was counteracted at 200 mm displacement by the system used to apply the load.

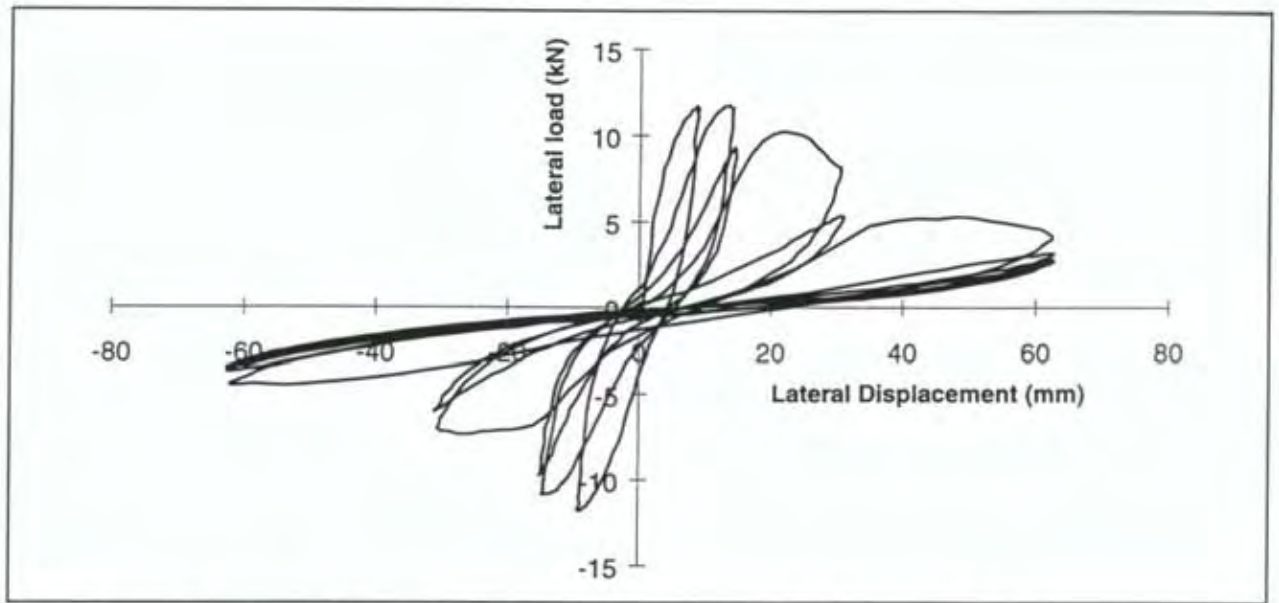


Figure B14 a) Load-displacement responses of Specimen LW2 during cyclic loading.

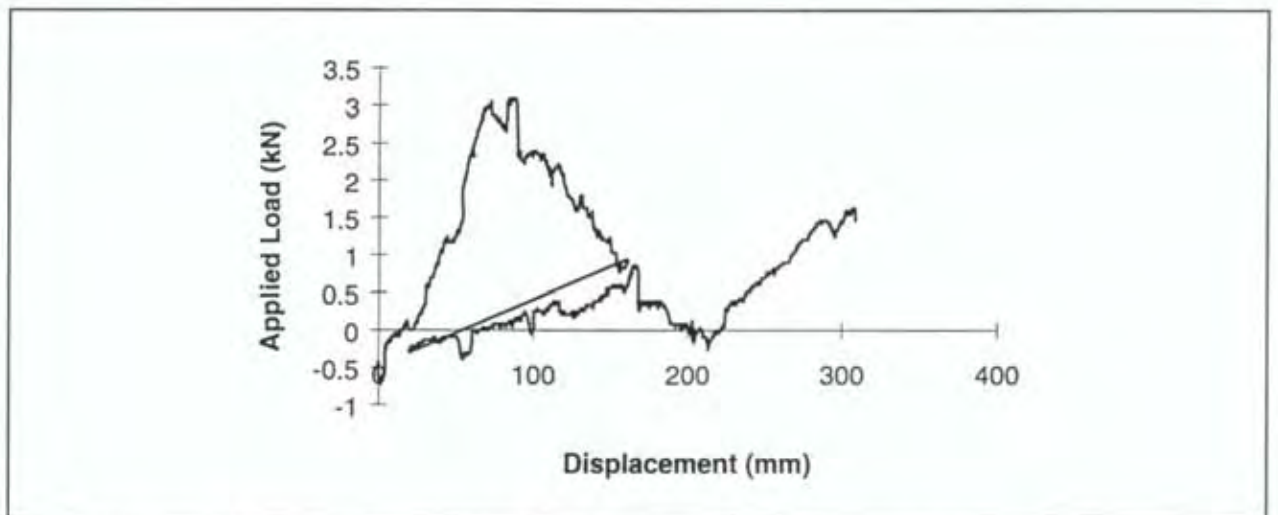


Figure B14 (continued) b) Load-displacement responses of Specimen LW2 during the push to failure.

Nailslip between the plasterboard and the perimeter framing members (measured close to the centre of and along the axis of the framing member) is given in Table B5.

Table B5 Perimeter Plasterboard Nailslip for Specimen LW2.

Cycle	Lateral		Plasterboard			
	Deflection (mm)	Load (kN)	Top (mm)	Bottom (mm)	Left (mm)	Right (mm)
+1	9.0	11.7	3.3	-3.1	0.4	-0.7
-1	-9.2	-11.8	-3.5	3.9	-1.1	1.0
+2	14.2	11.8	5.2	-5.9	1.0	-1.1
-2	-14.6	-10.9	-5.2	7.2	-1.6	1.4
+3	14.6	9.3	5.5	-6.7	1.1	-1.0
-3	-15.0	-9.7	-5.4	7.7	-2.2	1.4
+4	30.6	8.2	7.1	<-20	2.2	-1.6
-4	-30.6	-7.0	-4.7	24.5	-1.9	2.2
+5	31.0	5.4	5.5	-	2.2	-1.3
-5	-31.0	-6.1	-4.4	26.7	-3.2	2.1
+6	62.6	4.5	5.7	-	3.9	-2.8
-6	-62.1	-4.5	-4.1	>30	-3.6	2.9
+7	62.8	3.2	5.1	-	-	-2.8
-7	-62.4	-3.7	-4.0	-	-	2.9
+8	62.9	2.8	5.0	-	-	-2.6
-8	-62.1	-3.5	-4.0	-	-	2.8
+9	62.9	2.7	5.0	-	-	-2.6
-9	-62.4	-3.5	-4.0	-	-	2.8

The plot shown in Figure B15 compares the measured lateral displacement with displacements arising from two of the Figure B5 deformation modes, namely mode III (nailslip measured between the plasterboard and the top and bottom framing plates) and mode II (nailslip around the perimeter of the plasterboard). The remainder of the lateral displacement may be attributed to modes IV (rigid-body rotation measured by the left and right end stud uplift) and I (shear deformation of the plasterboard).

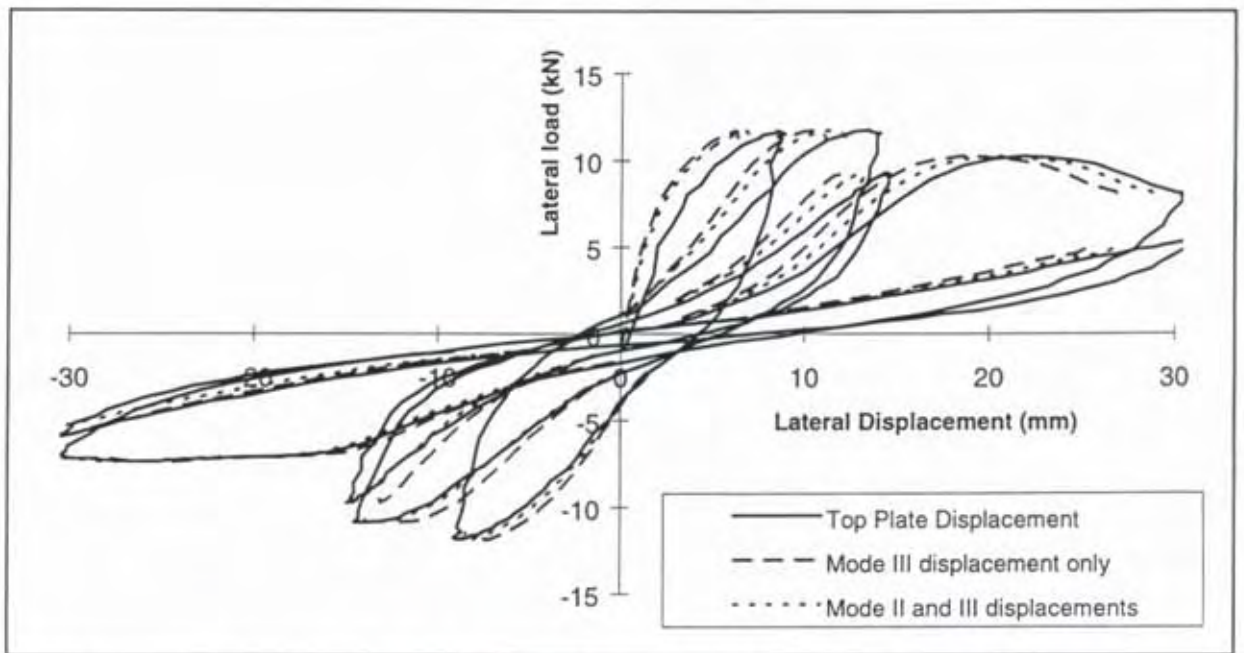


Figure B15 Lateral displacements compared to those arising from nailslip only.

B4. Specimen LW3

B4.1. Specimen LW3 Construction

Specimen LW3, intended to be representative of braced wall construction commonly used in New Zealand, had four 1.2 m long by 2.4 m high Type B plasterboard sheets. The plasterboard sheets were attached to the framing with 30×2.5 mm flat head galvanised nails spaced at 150 mm centres around the perimeter of each sheet. Nails around the perimeter of the wall had a proprietary steel washer between the nail head and the plasterboard.



Figure B16 Construction details for Specimen LW3.

B4.2. Specimen LW3 Schedule

The test schedule for Specimen LW3 is given in Table B6.

Table B6 Specimen LW3 Test Schedule.

Cycle	Target Lateral Deflection (mm)	Measured			
		Lateral Deflection (mm)	Lateral Load (kN)	Left Uplift† (mm)	Right Uplift† (mm)
+1	10	7.0	21.7	3.1	-1.5
-1	-10	-8.3	-24.0	-0.9	5.0
+2	15	11.5	32.3	5.4	-2.0
-2	-15	-13.4	-27.4	-1.1	9.2
+3	15	11.7	29.9	5.1	-1.9
-3	-15	-13.9	-26.3	-1.1	9.1
+4	24	20.3	36.7	11.1	-2.5
-4	-24	-22.4	-30.2	-1.4	17.5
+5	24	20.6	33.2	10.1	-2.3
-5	-24	-23.0	-27.8	-1.3	17.1
+6	36	33.2	38.5	17.4	-2.7
-6	-36	-30.0/- 35.0	-28.2/- 20.2	-1.5	24.1
+7	36	34.9	23.6	12.5	-2.4
-7	-36	-36.0	-18	-1.3	21.1
+8	36	35.5	17.8	12.5	-2.2
-8	-36	-35.9	-15.7	-1.2	20.7
+9	36	35.6	17.3	11.9	-2.2
-9	-36	-36.4	-14.9	-1.2	20.6
+10	36	35.3	16.6	11.2	-2.1
-10	-36	-36.5	-14.5	-1.2	20.4
+11	36	35.7	16.4	11.1	-2.1
-11	-36	-36.4	-14.0	-1.1	20.1
+12	60	59.8	20.2	26.3	-2.6
-12	-60	-72.9	-16.0	-1.4	38.3
+13	60	85.2	18.6	24.5	-2.5
-13	-60	-666.3	-14.5	-1.4	38.4
+14	90	90.9	18.2	38.3	-2.5
-14	-90	-92.3	-13.1	-1.2	61.1
+15	90	93.0	10.5	-	-
-15	-90	-93.3	-5.3	-	61.7

B4.3. Specimen LW3 Description

Cycle 1 ±10 mm	There was little sign of plasterboard damage around the nails after the ±10 mm cycle. The 3 to 5 mm uplift (see Table B6) at the wall ends was mostly due to the bottom framing plate separating from the flooring over a length of approximately 1 m from the wall end. This occurred because uplift arising from the lateral force of 22 to 24 kN exceeded the restraint provided by the gravity load.
Cycles 2 to 3 ±15 mm	There was some damage to the plasterboard around the nail heads in the two bottom corners of the wall during these two cycles. The end stud uplift increased to 5 to 10 mm with the bottom plate separating from the flooring over approximately a third of the wall length.
Cycles 4 to 5 ±24 mm	There was further plasterboard damage and nailslip to that observed in cycles 3 and 4 during these two cycles.
Cycles 6 to 11 ±36 mm	The vertical plasterboard sheet joint in the centre of the specimen fractured at a displacement of -30 mm during cycle -6 causing the load to decrease (see Table B6). The plasterboard nails in the centre stud were pulled completely through the plasterboard which was completely separated from the centre stud. The wall then behaved as two separate units for the remainder of the cycles.
Cycles 12 to 13 ±60 mm	The behaviour during these two cycles was essentially the same as the previous six with the exception that deformations were greater.
Cycles 14 to 15 ±90 mm	The deformations increased again and the plasterboard movements were greater, deforming as shown in Figure B17, with the left half of the plasterboard translating and the right half rotating. The left half of the plasterboard remained attached to the top half of the framing, inducing the greatest nailslip between itself and the bottom plate, whereas the right half of the plasterboard remained attached to the right end of the wall, inducing the greatest nailslip between itself and the centre stud.
Push to Failure	Most of the potentiometers were removed and the specimen was pushed to a total displacement of 150 mm. The behaviour described above was accentuated during this loading, as shown in Figure B18.

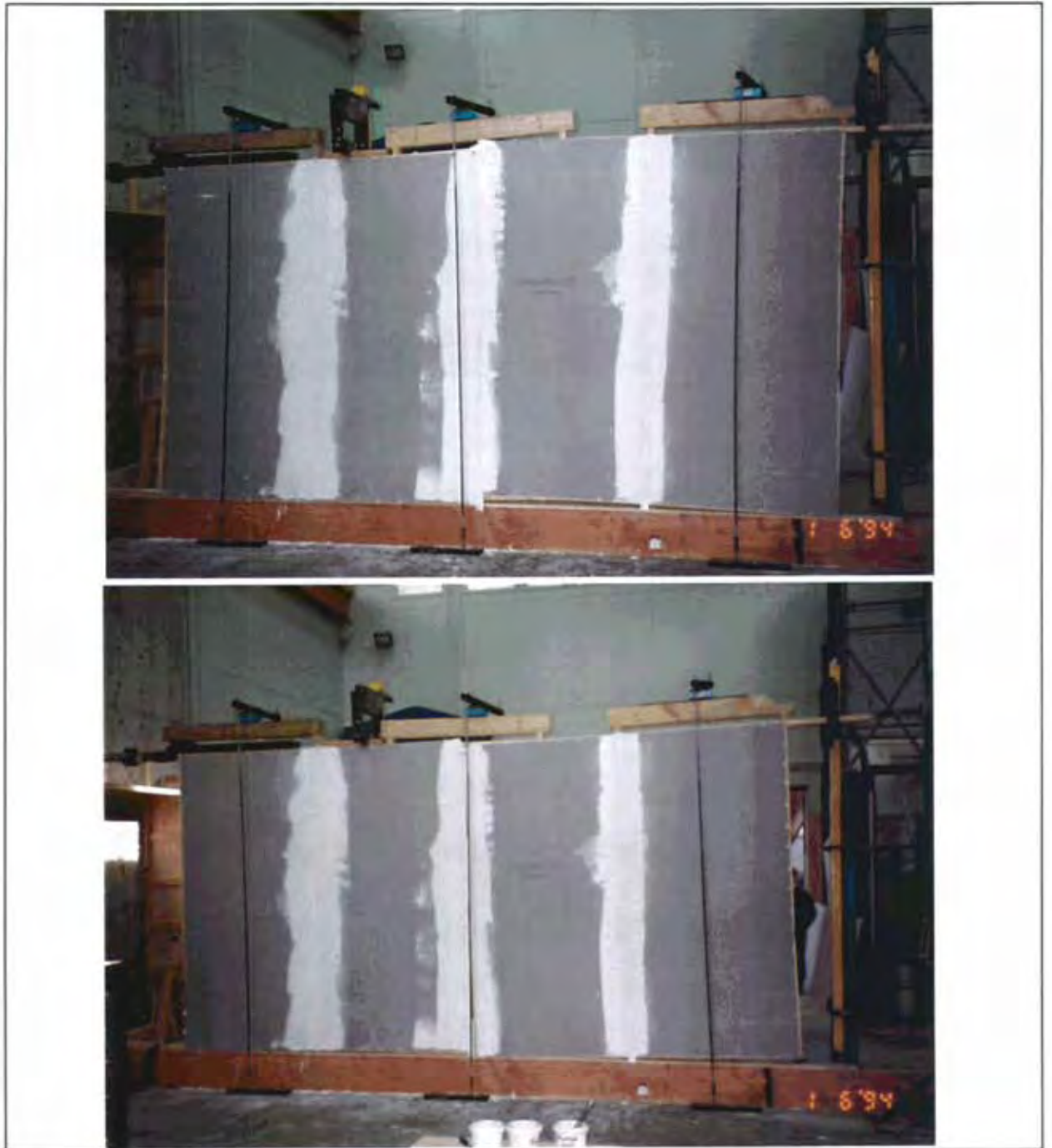


Figure B17 Specimen LW3 during cycles -13 (upper) and +14 (lower).



Figure B18 Specimen LW3 at the end of the test.

B4.4. Specimen LW3 Results

The load-displacement response of Specimen LW3 is given in Figure B19.

Nailslip between the plasterboard and the perimeter framing members (measured close to the centre of and along the axis of the framing member) is given in Table B7.

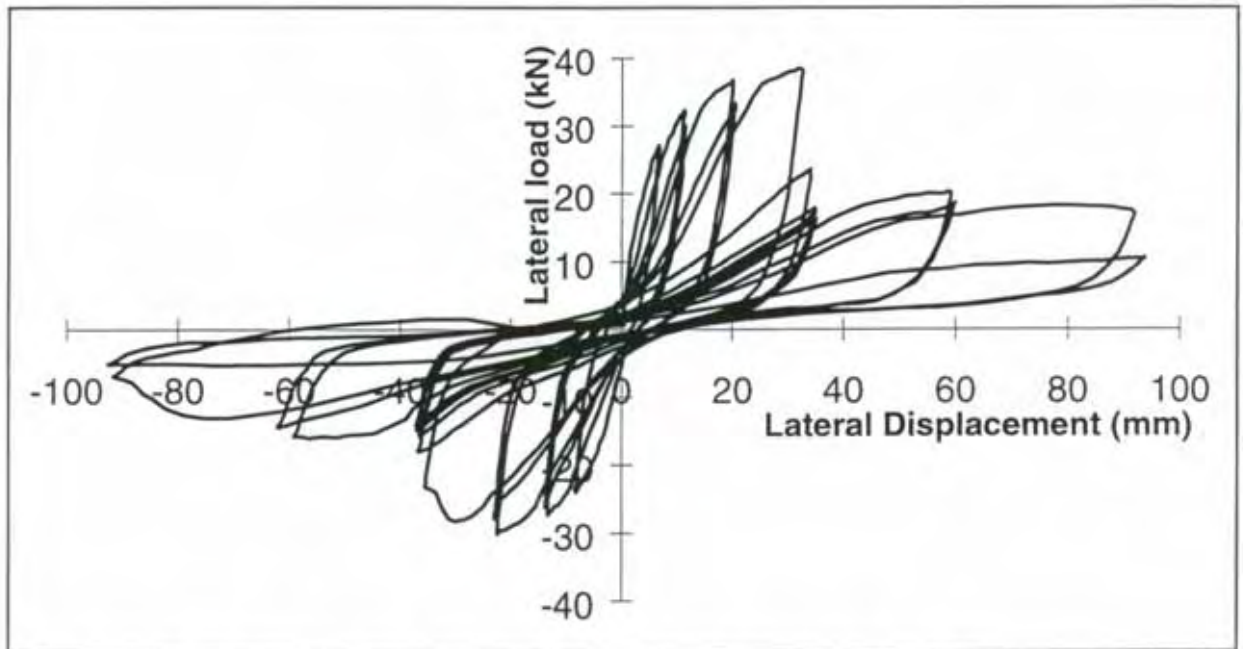


Figure B19 Load-displacement response of Specimen LW3.

Table B7 Perimeter Plasterboard Nailslip for Specimen LW3.

Cycle	Lateral		Plasterboard			
	Deflection (mm)	Load (kN)	Top (mm)	Bottom (mm)	Left (mm)	Right (mm)
+1	7.0	21.7	1.2	-1.7	0.2	-0.4
-1	-8.3	-24.0	-1.1	1.7	-1.3	-0.1
+2	11.5	32.3	2.3	-2.7	-0.4	-0.7
-2	-13.4	-27.4	-2.0	2.5	-2.2	-0.2
+3	11.7	29.9	2.5	-3.0	-0.6	-0.7
-3	-13.9	-26.3	-2.2	2.7	-2.3	-0.2
+4	20.3	36.7	4.0	-4.3	-0.6	-1.8
-4	-22.4	-30.2	-3.3	3.7	-3.8	-0.4
+5	20.6	33.2	4.4	-4.7	-0.9	-1.9
-5	-23.0	-27.8	-3.6	4.0	-4.0	-0.3
+6	33.2	38.5	6.7	-6.5	-	-3.2
-6	-35.0	-20.2	-5.7	4.7	-5.9	-0.6
+7	34.9	23.6	7.9	-7.5	-2.8	-3.4
-7	-36.0	-18	-5.9	3.9	-6.2	-0.7
+8	35.5	17.8	8.1	-7.3	-1.5	-3.5
-8	-35.9	-15.7	-5.8	3.7	-6.3	-0.5
+9	35.6	17.3	8.3	-7.3	-1.1	-3.5
-9	-36.4	-14.9	-5.8	3.8	-6.4	-0.4
+10	35.3	16.6	8.3	-7.2	-1.3	-3.6
-10	-36.5	-14.5	-5.7	3.8	-6.5	-0.4
+11	35.7	16.4	8.4	-7.3	-1.6	-3.6
-11	-36.4	-14.0	-5.7	3.9	-6.5	-0.4
+12	59.8	20.2	12.5	-9.1	-1.3	-4.7
-12	-72.9	-16.0	-6.3	5.1	-8.9	-0.4
+13	85.2	18.6	12.7	-8.7	-1.7	-5.0
-13	-666.3	-14.5	-6.1	5.2	-9.4	-0.4
+14	90.9	18.2	-	-	-1.8	-5.3
-14	-92.3	-13.1	-	-	<-10.0	-0.3
+15	93.0	10.5	-	-	-	-5.4
-15	-93.3	-5.3	-	-	-	-0.4

B5. Specimen LW4

B5.1. Specimen LW4 Construction

Specimen LW4 was constructed identically to Specimen LW1 except the plasterboard nail spacing was increased from 150 to 200 mm along the top framing plate in order to induce nail failure along that line of nails rather than along the bottom framing plate as the other three specimens had. This failure mode was desirable because the walls which failed in the Northridge earthquake failed along the top framing plate causing the sheet to fall off completely.

B5.2. Specimen LW4 Schedule

The test schedule for Specimen LW4 is given in Table B8.

Table B8 Specimen LW4 Test Schedule.

Cycle	Target Lateral Deflection (mm)	Measured			
		Lateral Deflection (mm)	Lateral Load (kN)	Left Uplift (mm)	Right Uplift (mm)
+1	8	6.1	16.2	2.6	-2.2
-1	-8	-5.6	-14.9	-2.3	2.8
+2	15	12.8	19.2	3.4	-2.5
-2	-15	-12.9	-15.0	-2.5	2.5
+3	15	13.9	10.5	-1.1	-2.0
-3	-15	-13.8	-9.4	-2.2	1.0
+4	24	23.7	7.7	-1.1	-1.8
-4	-24	-24.0	-2.8	-1.7	-1.2
+5	24	23.9	1.4	-1.5	-1.4
-5	-24	-24.1	-2.3	-1.8	-1.2

B5.3. Specimen LW4 Description

Cycle 1 ±8 mm	No visible damage to the specimen.
Cycles 2 to 3 ±15 mm	The plasterboard nails in the top framing plate were progressively withdrawn through the plasterboard during these two cycles until, at the end of cycle 3, the plasterboard was completely detached from the top framing plate. Wrinkling around the plasterboard paper face indicated that the plasterboard had also become detached from the top 0.5 to 0.8 m of the studs. The plasterboard nails pulled through the sheet edges over the top 0.8 m at each end of the specimen.
Cycles 4 to 5 ±24 mm	The specimen continued to deteriorate in a similar manner to that during cycles 2 and 3. There was a noticeable amount of curvature in the uppermost portions of the studs.
Push to Failure	The position of the maximum stud curvature moved down the stud as the glue attaching the stud to the plasterboard progressively ruptured until, at 150 mm displacement, all except the left end stud were no longer attached to the plasterboard. The specimen is shown at 60 and 120 mm displacements in Figure B20.

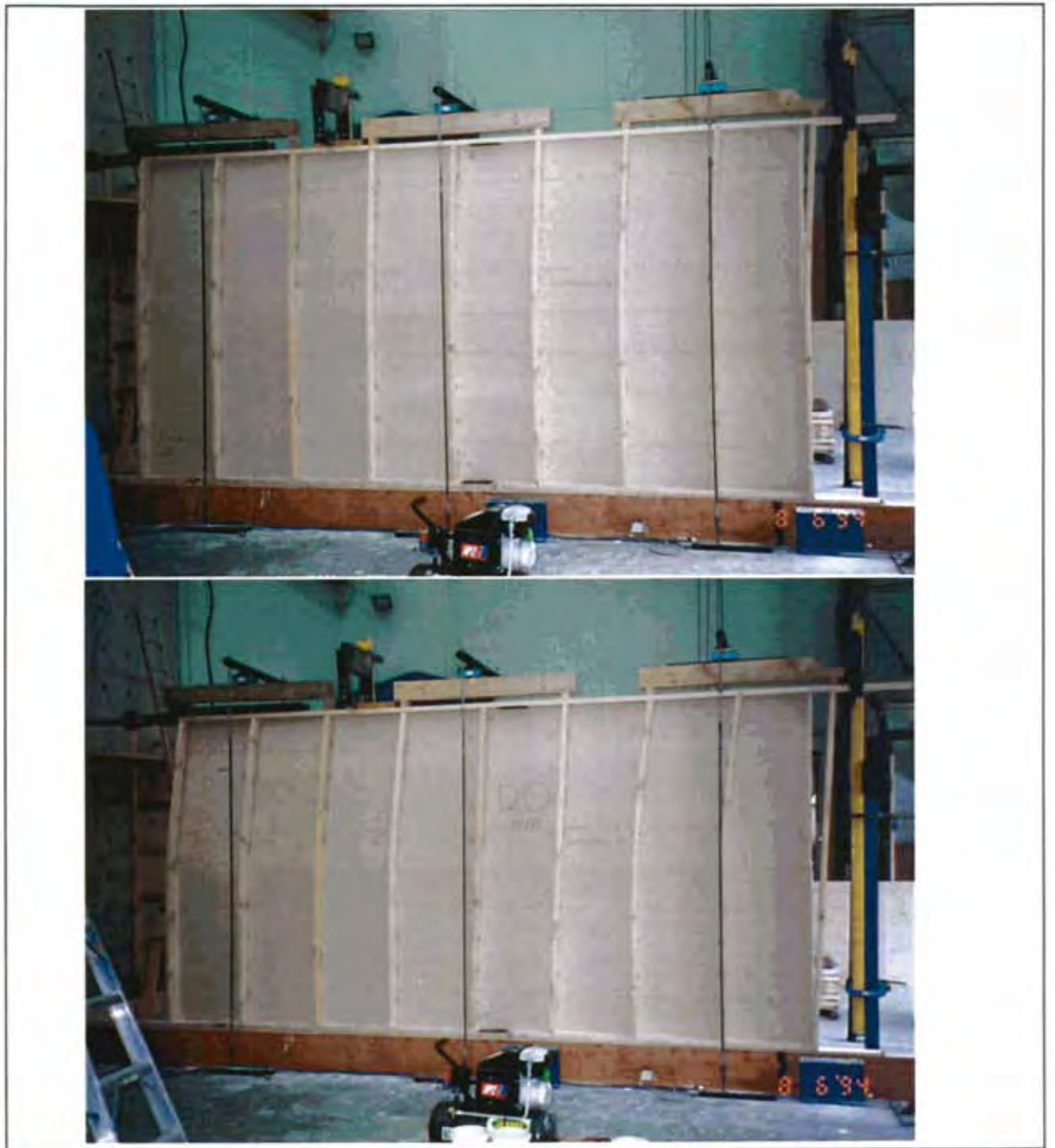


Figure B20 Specimen LW4 at: a) 60 mm and b) 120 mm displacement.

B5.4. Specimen LW4 Results

The load-displacement response of Specimen LW4 is given Figure B21.

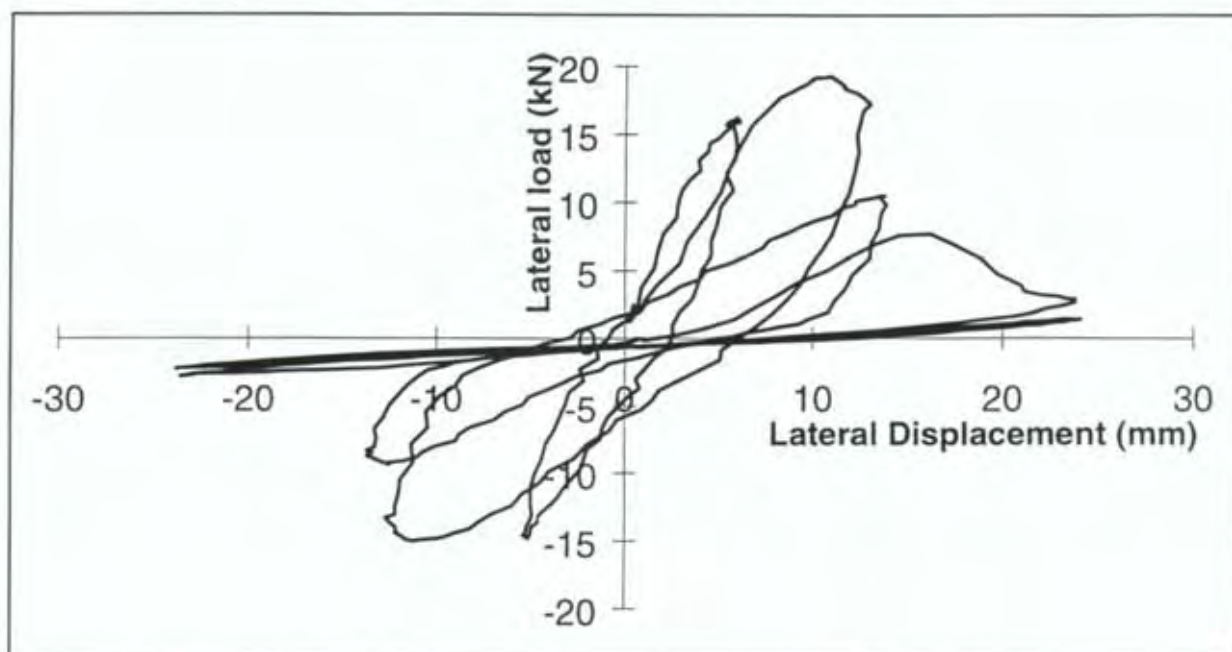


Figure B21 Load-displacement response of Specimen LW4.

Nailslip between the plasterboard and the perimeter framing members (measured close to the centre of and along the axis of the framing member) is given in Table B9.

Table B9 Perimeter Plasterboard Nailslip for Specimen LW4.

Cycle	Lateral		Plasterboard			
	Deflection (mm)	Load (kN)	Top (mm)	Bottom (mm)	Left (mm)	Right (mm)
+1	6.1	16.2	1.4	-1.6	0.3	-0.2
-1	-5.6	-14.9	-1.2	1.4	0.3	0.1
+2	12.8	19.2	5.7	-2.9	0.6	-0.4
-2	-12.9	-15.0	-8.0	1.9	0.6	0.3
+3	13.9	10.5	9.5	-2.1	0.7	0.2
-3	-13.8	-9.4	-10.8	1.4	0.7	0.4
+4	23.7	7.7	21.5	-1.7	1.0	0.3
-4	-24.0	-2.8	-21.4	0.2	1.1	0.6
+5	23.9	1.4	-	-0.6	-	-
-5	-24.1	-2.3	-	-0.2	-	-

B6. Experimental Specimen Comparison

Envelopes of the load-displacement responses of the four specimens are reproduced on the same axis in Figure B22 for strength and stiffness comparisons.

Specimen LW3 had the greatest stiffness and strength and Specimen LW2 had the least stiffness and strength. This difference may be attributed to Specimen LW3 having a greater number of nails (i.e. a smaller nail spacing) around the perimeter of the sheathing than Specimen LW2. (Washers beneath the nail heads also increase the strength, stiffness and ductility of nailed joints.)

The two glued specimens (LW1 and LW4) were also stiffer and stronger than Specimen LW2. This reflected the sheathing movement relative to the framing, which was mostly translational in the glued specimens but comprised translation and rotation in Specimen LW2.

The peak loads were applied to Specimen LW3 at displacements of +33 and -30 mm. These displacements were significantly greater than those of the other specimens at their peak loads. This reflected the additional nail displacement capacity produced by the introduction of washers beneath the nail heads.

The two glued specimens (LW1 and LW4) exhibited brittle failure whereby the load dropped immediately after the glue ruptured and was unrecoverable during cycles to greater displacements. The two nailed only specimens (LW2 and LW3) exhibited reserve strength whereby the strength recovered during cycles to greater displacements.

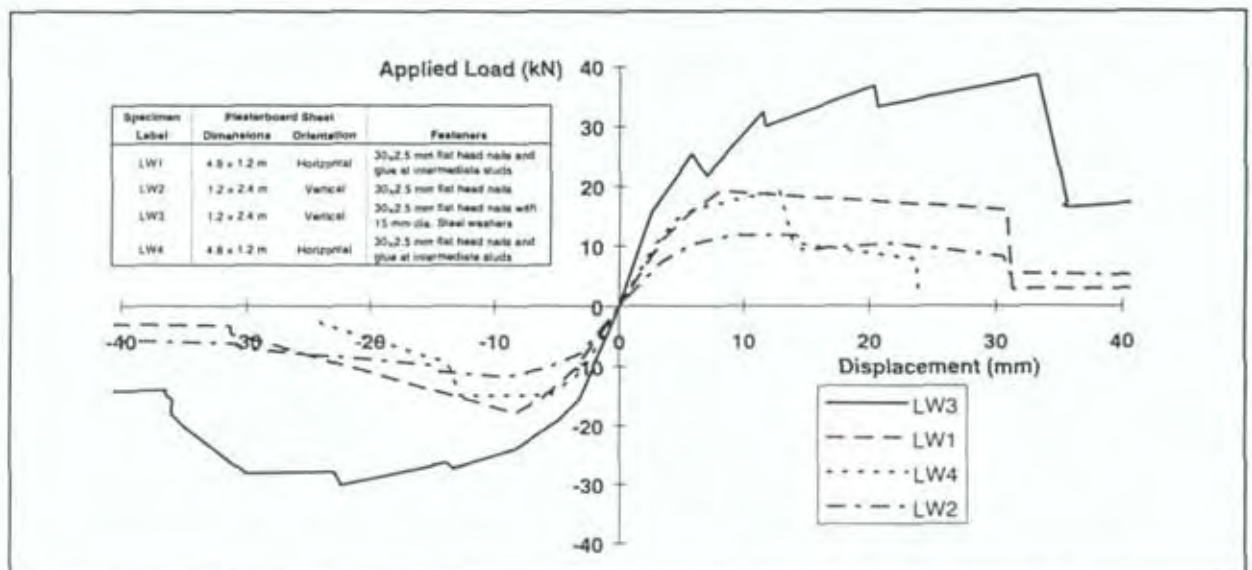


Figure B22 Load-displacement response envelopes for Specimens LW1 to LW4.

The responses of specimens LW1 and LW4 were similar, indicating repeatable results, although specimen LW4 was able to sustain more load at 14 mm deflection than specimen LW1. This was attributed to use of a 6mm first cycle displacement (compared to 8 mm for LW1), which caused less nail degradation.

B7. Conclusions

The glued specimens were not able to sustain load at the same displacements as the nailed specimens because the glue restrained rotation of the sheathing material, forcing premature failure of one line of nailed fasteners.

Strength, stiffness and ductility were greater when washers were used with the nails.

All of the specimens eventually failed through the deterioration of one line of nailed fasteners. This highlighted the need for correct detailing of components so they degrade in a controlled and predictable manner.

The nailed connection between the sheathing and bottom framing plate usually degraded first although this was able to be prevented by increasing the nail spacing in the top plate which then caused these nails to degrade first.

The sheet orientation (i.e. horizontal or vertical) did not affect the behaviour of the test specimens except where the sheet joints ruptured (at large loads and displacements).

While vertical gravity load did not cause instability of the test specimens, there was sufficient degradation for instability to occur if greater displacements were imposed (as would almost certainly be the case in an earthquake or during aftershocks).

APPENDIX C: PROPRIETARY PRODUCTS USED IN THE RESEARCH

Two proprietary sheathings were used in the experimental programme described in this report.

One gypsum plasterboard was nominal 9.5mm standard Gib[®] plasterboard supplied by Winstone Wallboards Limited.

The other gypsum plasterboard was nominal 9.5mm Gib[®] BRACELINE plasterboard supplied by Winstone Wallboards Limited. The proprietary nails and washers used to fasten the Gib[®] BRACELINE to the timber framing were also supplied by Winstone Wallboards Limited.

Note: Results obtained in this study relate only to the samples tested, and not to any other item of the same or similar description. BRANZ does not necessarily test all brands or all types available within the class of items tested, and exclusion of any brand or type is not to be taken as any reflection on it.

This work was carried out for specific research purposes, and BRANZ may not have assessed all aspects of the products named which would be relevant in any specific use. For this reason, BRANZ disclaims all liability for any loss or other deficit, following use of the named products, which is claimed to be based on reliance on the results published here.

Further, the listing of any trade or brand names above does not represent endorsement of any named product nor imply that it is better or worse than any other available product of its type. A laboratory test may not be exactly representative of the performance of the item in general use.



BRANZ MISSION

To be the leading resource for the development of the building and construction industry.

HEAD OFFICE AND RESEARCH CENTRE

Moonshine Road, Judgeford
Postal Address - Private Bag 50908, Porirua
Telephone - (04) 235-7600, FAX - (04) 235-6070

REGIONAL ADVISORY OFFICES

AUCKLAND

Telephone - (09) 526 4880
FAX - (09) 526 4881
419 Church Street, Penrose
PO Box 112-069, Penrose

WELLINGTON

Telephone - (04) 235-7600
FAX - (04) 235-6070
Moonshine Road, Judgeford

CHRISTCHURCH

Telephone - (03) 366-3435
FAX (03) 366-8552
GRE Building
79-83 Hereford Street
PO Box 496